To be published in the Proceedings of the ASME Turbo Expo 2011, June 6-10, 2011, Vancouver, Canada.

Proceedings of ASME Turbo Expo 2011
GT2011
June 6-10, 2011, Vancouver, Canada

GT2011-46583

TEST CONDITIONS FOR PERFORMANCE CHARACTERIZATION OF DIELECTRIC BARRIER DISCHARGE (DBD) PLASMA ACTUATORS FOR ACTIVE FLOW CONTROL IN JET ENGINES

David E. Ashpis
National Aeronautics and Space Administration
Glenn Research Center
Cleveland, Ohio, USA
ashpis@nasa.gov

Douglas R. Thurman
United States Army Research Laboratory
Glenn Research Center
Cleveland, Ohio, USA
drthurman@nasa.gov

ABSTRACT

Dielectric Barrier Discharge (DBD) plasma actuators for active flow control in the jet engine need to be tested in the laboratory to characterize their performance at flight operating conditions. DBD plasma actuators generate a wall-jet electronically by creating weakly ionized plasma, therefore their performance is affected by gas discharge properties, which in turn depend on the pressure and temperature at the actuator placement location. Characterization of actuators is initially performed in a laboratory chamber without external flow. It is usually impractical to simultaneously set engine pressures and temperatures in a chamber, and a simplified approach is desired. It is assumed that the plasma discharge depends only on the gas density. Other temperature effects are assumed to be negligible. Therefore, tests can be performed at room temperature with chamber pressure set to yield the same density as in engine operating flight conditions. Engine data was obtained from four generic engine models; 300-, 150-, and 50-Passenger (PAX) aircraft engines, and a military jet-fighter engine. The static and total pressure, temperature, and density distributions along the engine were calculated for sea-level takeoff and altitude cruise, and the chamber pressures needed to test the actuators were calculated. The results show that testing has to be performed over a wide range of pressures from 12.4 to 0.03 atm, depending on the application. For example, if a DBD plasma actuator is to be placed at the compressor exit of a 300 PAX engine, it has to be tested at 12.4 atm for takeoff, and 6 atm for cruise conditions. If it is to be placed at the low-pressure turbine, it has to be tested at 0.5 and 0.2 atm, respectively. These results have implications for the feasibility and design of DBD plasma actuators for jet engine flow control applications. In addition, the distributions of unit Reynolds number, Mach number, and velocity along the engine are provided. The engine models are non-proprietary and this information can be used for evaluation of other types of actuators and for other purposes.

NOMENCLATURE

H	Altitude
M	Mach number
P	Static pressure
R	Gas constant
Rey	Reynolds number
T	Static temperature
V	Velocity
X	Axial distance along the engine
ρ	Density

Subscripts

c	Conditions in chamber

INTRODUCTION

There is strong interest in active flow control techniques for applications in the jet engine, for example, to eliminate flow separation, improve efficiency or reduce noise [1]. Dielectric Barrier Discharge (DBD) Plasma actuators were proposed for active flow control of various flows, and the technology has been an active research area in the last decade.

The main active flow control technique in aerodynamics is based on injection of small jets in a steady or unsteady manner into the flow. The small input creates a large global effect that

PREPRINT - DO NOT DISTRIBUTE - FOR INTERNAL USE ONLY

provides the desired flow improvement. DBD plasma actuators create a wall-jet by purely electronic means. The jet can be steady, or in unsteady mode by pulsing or modulating, and can be used for active flow control, similar to any pneumatically- or mechanically-generated jet.

A DBD actuator is shown in Fig. 1. The actuator consists of a pair of thin conducting electrodes separated by a dielectric. Usually there is one exposed electrode and one covered electrode and the electrodes are offset. Typically, at atmospheric conditions, a high voltage (1 to 40 kV RMS), high frequency (1 to 20 kHz), signal is applied to the electrodes, creating localized weakly ionized gas plasma discharge on the surface near the edge of the exposed electrode. A typical discharge is shown in Fig. 2.

The jet is generated in the plasma region via the electrohydrodynamic effect, a process of collisions between ions and neutral molecules in the plasma. The actuator construction is very simple, but the physical mechanisms involved are quite complex and include interactions among electrical fields, electrons, positively and negatively charged species, the electrodes, and the dielectric surface [2 to 4]. Gas is drawn from the surroundings to form a thin wall jet that is roughly parallel to the surface and directed away from the exposed electrode edge in the direction of the covered electrode, as visualized by experiments and computation [5 to 7]. There is slight heating involved, but its effect on the jet is negligible. Other types of plasma-based flow control devices that generate localized intense heating [8] are not included in the scope of devices addressed in this paper. More detailed information and references on DBD actuators and their applications for aerodynamic flow control can be found in several review articles including [9 to 12].

The advantages of DBD actuators are that they are surface-mounted, fully electronic, low power, high frequency-band devices. There are no moving parts, tubes, ducts or surface holes. Flexible operation is possible by controlling the input voltage and waveforms. DBD plasma actuators are particularly attractive for gas turbine and turbomachinery applications: They are thin, surface mounted, and do not require internal volumes or passages. Their construction can be made suitable for high temperature environment by choosing high-temperature alloys for the electrodes and temperature-resistant ceramic materials for the dielectric. They can easily be integrated with futuristic engine components to be made of ceramics and composites.

The majority of the research in DBD actuators area was focused on applications in external flows, particularly for wings and airframes, rather than on propulsion. But there have been important efforts directed to turbomachinery applications. There have been several successful experimental demonstrations of active flow control with DBD plasma actuators to eliminate low Reynolds number separation in Low-Pressure Turbine flows [13 to 16], and to reduce effects of turbine tip leakage [17 to 20]. Those experiments were performed in wind tunnels or linear cascades at room temperature.

DBD actuators need to be tested in actual flight conditions in order to be used as flow control devices in practical applications. Some flight tests were performed on air vehicles; on a small remotely controlled airship [21, 22], a full-size piloted glider [23], and a small UAV [24], but no tests have been performed in jet engines. The aerodynamic performance of the actuators needs to be characterized to prove that they have sufficient authority at the flow conditions at the location of their placement in the jet engine. In addition, the electrical performance, particularly the power consumption of the actuators, needs to be quantified, as it is needed for design of power supplies and for cost-benefit analysis of the flow control technology. This paper addresses the test conditions needed to characterize the actuators in the laboratory.

The basic characterization in the laboratory is performed without external flow. The aerodynamic performance is characterized by measuring the velocity profile of the wall jet and/or the thrust generated by the actuator. The electrical performance is characterized by measuring the current, voltage and power. Most of the tests to date have been performed at room temperature and atmospheric conditions, but in order to simulate flight conditions the actuator has to be placed in a chamber with controlled temperature and pressure representative of the flow conditions in flight. A small number of tests are reported in the literature in chambers at room temperature and sub atmospheric conditions, with some conflicting results [25 to 32]. Tests at atmospheric altitude conditions have been performed in an environmental chamber [33], where temperature and pressure were varied simultaneously. These tests were mostly motivated by aerodynamics applications. Tests at above-atmospheric pressures at room temperature were reported in [34, 35] and provide information relevant to internal flow applications.

The applications of interest here are in the jet engine, and, therefore, the actuator performance has to be tested in conditions that simulate the operating conditions in flight, at the location where the actuator is placed. But it is challenging to simultaneously replicate the pressures and elevated temperature conditions of the jet engine in a chamber. It is desirable to find a simpler approach to eliminate this technical complication. The question that arises is how to simulate the conditions in an operating jet engine in order to test the actuators. The answer is anchored in the physics of the DBD plasma and can simplify the testing. Because the principle of operation of DBD actuators depend on electrical discharges and on the associated force generation mechanisms, the performance of the actuator will be affected by the pressure, temperature and properties of the gas. It is assumed that for the range of temperatures in the jet engine, the gas density alone is the significant gas property influencing the performance of the actuator. Therefore the flight conditions can be simulated by matching the density in the laboratory. It is a simple idea that was not proposed before.

The outline of this paper is as follows. First, information is provided on pressure, temperature, density, velocity, Mach number and unit Reynolds number distribution along the stations of four typical jet engines. This information is derived

from non-proprietary models of engines used in system analysis studies by NASA. These models include cycle, flow path and sizing. Then, by setting the chamber pressure at room temperature, the density is matched to the operating conditions in flight. The range of the needed chamber pressures was calculated. It depends on the placement of the actuator, and the results are presented for the four typical engines at takeoff and cruise conditions. This information is useful to serve as a guideline for testing requirements of DBD plasma actuators at engine flight conditions. The engine information documented here, which is often hard to find in publically available sources, is useful for evaluation of other types of actuators as well as for other purposes.

JET ENGINE DATA SOURCE—ENGINE MODELS

The engine models used in this study were developed based on information available in open literature and empirical estimates. Cycle analysis was performed with the Numerical Propulsion Simulation System (NPSS) code [36, 37], providing performance parameters such as thrust, component pressure ratios, and velocities, temperatures, and pressures at each engine station. Aeromechanical analysis and estimates of engine and component weights were calculated using the Weight Analysis of Turbine Engines (WATE) code [38], which also provides a flow path schematic of the engine. Engine models were developed for a total of four generic engine types: 300-, 150- and 50-passenger (PAX) aircraft engines, and a military jet-fighter engine. The models are a good representation of actual engines. The primary engine parameters of thrust, weight, overall pressure ratio, and bypass ratio are listed in Table 1 and the schematic of each engine is shown in Fig. 3. The axial coordinates of the components outflow planes are listed in Table 2.

Engine conditions were calculated at the inlet and exit planes of the various engine components. Variable gas thermodynamic properties were used in the calculations. Data was acquired for two engine operating conditions: sea-level takeoff and altitude cruise at 35,000 ft. Data for the 50 PAX engine is also shown for an additional cruise altitude of 65,000 ft, as this type of engine is also used for high flying air vehicles. Figures 4 to 7 show the following parameters for each engine: static and total (stagnation) pressure, temperature, and density, unit Reynolds number, Mach number, and velocity. Ideal gas conditions were assumed. For all data shown, the flight Mach numbers are M = 0.8 at cruise and M = 0 at takeoff. Figure 6(d) for the 50 PAX engine also shows the unit Reynolds number for cruise Mach numbers of M = 0.5, 0.6, and 0.8 at altitude of 65,000 ft. The figures show the variation of the various parameters as a function of the axial distance X along the engine. An annotated schematic of the engine accompanies every figure to help in identification of the various stations.

There is more data presented than is strictly needed for development of the subject test conditions. The motivation for including the extra data is to make it available to the research community because it is hard to find non-proprietary actual engine data. The engine data presented here is unrestricted and can be used for other purposes.

TEST CONDITIONS FOR DBD PLASMA ACTUTORS

Several assumptions are used to develop the test conditions in laboratory experiments in quiescent environment (no flow) in a chamber:

(a) The effect of temperature and pressure on plasma kinetics and chemistry is ignored. This assumption is reasonable for the range of temperatures in the jet engines, and is further discussed below.
(b) The effect of temperature on the electrical properties of the actuator, particularly on the capacitance of the dielectric, is negligible. The capacitance variation was calculated by [33], and was shown to be small.
(c) Actuator heat generation is negligible. This assumption is based on experimental observations for the range of power and voltages applied to conventional DBD plasma actuators.
(d) Gas composition effects are ignored. There is a small effect of the composition of the atmosphere variation with altitude mainly due to variation of the oxygen/nitrogen ratio [32]. Potentially there may be an effect due to the presence of combustion products in the areas of the engine downstream of the combustors. For simplicity these effects are assumed to be insignificant.
(e) Gas thermodynamic properties are constant (except in the engine model data calculations).

The main assumption is that the gas density number is the only parameter that governs the physical process of the jet generation by the plasma discharge. A process of collisions between ions and neutral molecules create the forces that result in the jet. The collisions are governed by the mean-free-path and the number of molecules in a unit volume. Therefore, with the assumptions listed above, the gas density in laboratory tests should be the same as the density at the application flight conditions.

Assessment of the validity of these assumptions and possible subsequent refinements is a subject of future work. With these assumptions, the main factor affecting the jet generation dependence on pressure and temperature is captured by considering only the density, therefore, the conclusions provide at least a very good approximation.

Validation of the assumption that temperature affects only the density is not trivial. It is known that some of the reactions between different charged molecules and electrons in the plasma are temperature dependent. Usually the dependence is weak except for the temperature dependence of electron attachment processes, which can be significant above 1800 °R (1000 K). It seems that the only practical approach to assess the full effect of temperature and pressure on the momentum transferred to the fluid is to use numerical simulation of the DBD plasma actuator at different densities and pressures. This

simulation is challenging and is planned to be performed in the future. The authors are not aware of any reported work on this topic.

The assumption that the temperature affects only the density is very reasonable for temperatures under 1800 °R (1000 K). The open question is if it is significant at higher temperature levels. If it turns out that there is divergence from this assumption at all, it is expected to affect the calculated test conditions only for applications in the combustion chamber and the high-pressure turbine, which are at temperatures higher the 1800 °R, as seen from Figs. 4 to 7.

The chamber pressure and temperature to yield the same density as in flight is calculated as follows.

The gas density in the laboratory test chamber should be the same as the density at the application flight conditions,

$$\rho_c = \rho$$

where subscript c indicates conditions in the chamber.
Assuming an ideal gas with constant R,

$$\rho = P / RT$$

the following relationship is obtained

$$P_c = \frac{P}{\left(T / T_c\right)}$$

where

P_c, T_c, ρ_c – Laboratory chamber pressure, temperature, and density.

P, T, ρ – Static pressure, temperature and density at flight conditions.

The chamber pressures were calculated from the engine model data for the four generic engines. In the calculations sea-level pressure was 17.7 psi. Sea-level temperature was 545.7 °R (29.8 °C). This was also the value of the chamber room temperature. The results are displayed in Fig. 8.

DISCUSSION

The results show that the test chamber pressure varies greatly, from sub-atmospheric to above atmospheric pressures, depending on the operating conditions and location of the placement of the actuator in the engine. For example, if a DBD plasma actuator is to be placed at the inlet to the high pressure turbine for the 300 PAX engine, it has to be tested at 6 atm if it is intended to operate at sea-level takeoff conditions, and at 2.9 atm if it is intended to operate at 35,000 ft cruise. If it is to be used in the exit of high-pressure compressor duct (burner inlet) it has to be tested at 12.4 atm at takeoff conditions, and at 6.2 atm at 35,000 ft cruise conditions. If it is to be used at the low-pressure turbine exit, it has to be tested at 0.5 atm for operation at takeoff and at 0.2 atm at cruise. If the actuator is to be placed on the low-pressure turbine of the 50 PAX engine flying at 65,000 ft, its performance has to be tested at a very low chamber pressure of 0.03 atm.

Note that the calculations are based on conditions at the inflow and outflow planes of the various engine components. The calculated points are connected with straight lines. Further modification is needed to account for local flow conditions inside the component. For example, in turbomachinery there are inter-row and inter-stage variations, and in inter-blade passages there is acceleration or diffusion or even shock waves that will modify the results. Those local modifications are not included in this study and are left for future work.

Note also that the results shown in Fig. 8 display the chamber pressures based on total (stagnation) as well as static conditions in the engine. The reason that the results corresponding to total condition are shown is that the total conditions are equal to static condition at locations where the velocity is zero, corresponding to placement of the actuator at locations such as the leading edge of a turbine or compressor airfoil. As can be seen in the figure, the differences are not large.

Additional insights can be gained from the distribution of the unit Reynolds number. Usually low unit Reynolds number may indicate flow separation. For example, it is known that there is a flow separation problem on the low pressure turbine (LPT) at altitude. Those locations are good candidates for implementation of active flow control. However, those locations are also characterized by low density, requiring the plasma actuator to be tested at low chamber pressures. DBD plasma actuators may suffer from loss of performance as the pressure is decreased (note that there are insufficient and conflicting results in published literature). Therefore, laboratory testing is critical to establish that the DBD actuators can perform adequately under those conditions.

It is important to note that in the field of weakly ionized plasma research, laboratory experiments were traditionally performed in a vacuum chamber at room temperature. It therefore became common in that field to specify the chamber pressure as an experimental parameter. This may have led to habitually considering the pressure, rather than the density, as the relevant parameter.

CONCLUSIONS

Data on flow conditions in four generic jet engines was presented, and because it is non-restricted, the data is useful for various applications related to formulating test conditions of flow control devices placed in different engine components. The data was used to develop test conditions for characterization of DBD plasma actuators in a chamber at room temperature. The underlying assumption is that the performance of DBD actuators depends only on the density and that all other temperature-related effects are negligible at the temperature range existing in the jet engine. Based on this assumption and the engine models data, the pressure needed to

be set in the test chamber to simulate operating conditions in the engine was calculated. The pressures vary with the placement of the actuator in the engine, the type of engine, and the flight operating conditions. There is a wide spread in the pressure range, depending on the specific application, and can vary from 12.4 to 0.03 atm for the four engine models and flight conditions considered.

ACKNOWLEDGMENTS

This project was supported by the NASA Subsonic Fixed Wing Project of the Fundamental Aeronautics Program. We wish to thank Scott Jones and Michael Tong from NASA GRC for their help in developing the engine models. Thanks also to M. Shneider (Princeton University), A. Starikovskiy (Princeton University) and A. Likhanskii (Tech-X Corporation) for useful discussions on temperature effects on DBD plasma.

REFERENCES

[1] Lord, W.K., MacMartin, D.G., and Tillman G., 2000, "Flow Control Opportunities in Gas Turbine Engines," AIAA–2000–2234.

[2] Likhanskii, A.V., Shneider, M.N., Macheret, M.O., and Miles, R.B., 2006, "Modeling of Interaction Between Weakly Ionized Near-Surface Plasmas and Gas Flow," AIAA–2006–1204.

[3] Likhanskii, A.V., Shneider, M.N., Opaits, D.F., Miles, R.B., and Macheret, S.O., 2007, "Numerical Modeling of DBD Plasma Actuators and the Induced Air Flow," AIAA–2007–4533.

[4] Likhanskii, A.V., 2009, "Study of Plasma Phenomena at High Electric Fields in Applications for Active Flow Control and Ultra-Short Pulse Laser Drilling," Ph.D. Dissertation, The Pennsylvania State University, College Station, PA.

[5] Corke, T.C., Jumper, E.J., Post, M.L., Orlov, D., and McLaughlin, T.E., 2002, "Application of Weakly-Ionized Plasmas as Wing Flow-Control Devices," AIAA–2002–350.

[6] Suzen, Y.B., Huang, P.G., Jacob, J.D., and Ashpis, D.E., 2005, "Numerical Simulations of Plasma Based Flow Control Applications," AIAA–2005–4633.

[7] Suzen, Y.B., Huang, P.G., and Ashpis, D.E., 2007, "Numerical Simulations of Flow Separation Control in Low-Pressure Turbines Using Plasma Actuators," AIAA–2007–937.

[8] Samimy, M., Adamovich, I., Webb, B., Kastner, J., Hileman, J., Keshav, S., and Palm, P., 2004, "Development and Characterization of Plasma Actuators for High Speed and Reynolds Number Jet Control," Experiments in Fluids, 37 (4), 2004, pp. 577–588.

[9] Moreau, E., 2007, "Airflow Control by Non-Thermal Plasma actuators," J. Phys. D: Appl. Phys. 40 (2007) pp. 605–636.

[10] Corke, T.C., Post, M.L., and Orlov, D.M., 2007, "SDBD Plasma enhanced Aerodynamics: Concepts, Optimization and Applications," Progress in Aerospace Sciences 43 (2007) pp. 193–217.

[11] Corke, T.C., Post, M.L., and Orlov, D.M., 2009, "Single Dielectric Barrier Discharge Plasma Enhanced Aerodynamics: Physics, Modeling and Applications," Exp Fluids (2009) 46:1–26.

[12] Corke, T.C., Enloe, C.L., and Wilkinson, S.P., 2010, "Dielectric Barrier Discharge Plasma Actuators for Flow Control," Annu. Rev. Fluid Mech. 2010. 42:505–29.

[13] Hultgren, L.S., and Ashpis, D.E., 2003, "Demonstration of Separation Delay with Glow-Discharge Actuators," AIAA–2003–1025.

[14] List, J., Byerley, A.R., McLaughlin, T.E., and VanDyken, R.D., 2003, "Using a Plasma Actuator to Control Laminar Separation on a Linear Cascade Turbine Blade," AIAA–2003–1026.

[15] Huang J., Corke T.C., and Thomas F.O., 2006, "Plasma Actuators for Separation Control of Low Pressure Turbine Blades," AIAA J. 44:51–57.

[16] Huang J., Corke T.C., and Thomas F.O., 2006, "Unsteady Plasma Actuators for Separation Control of Low-Pressure Turbine Blades," AIAA J. 44:1477–87.

[17] Morris, S.C., Corke, T.C., VanNess, D., Stephens, J., and Douvillev, T., 2005, "Tip Clearance Control Using Plasma Actuators," AIAA–2005–782.

[18] VanNess, D.K., Corke, T.C., and Morris S.C., 2006, "Turbine Tip Clearance Flow Control Using Plasma Actuators," AIAA–2006–21.

[19] Douville, T., Stephens J., Corke T., Morris S., 2006, "Turbine Blade Tip Leakage Flow Control by Partial Squealer Tip and Plasma Actuators," AIAA–2006–20.

[20] VanNess, D.K., Corke, T.C., and Morris S.C., 2008, "Tip Clearance Flow Visualization of a Turbine Blade Cascade with Active and Passive Flow Control," ASME Paper No. GT2008-5070.

[21] Göksel, B., Fischer, M., Rechenberg, I., and Thallemer, A., 2005, "Elektrostatischer Plasma-Wellantrieb für Bionische Luftschiffe," Proceedings of the German Aerospace Congress 2005, Friedrichshafen, Germany, Deutsche Gesellschaft für Luft- und Raumfahrt Paper No. DGLR-2005-261, Vol. 3, pp. 1853–1856.

[22] Göksel, B., 2008, Private Communication, http://www.electrofluidsystems.com/airfish/b-ionic-airfish-2008.wmv

[23] Sidorenko, A., Budovsky, A., Pushkarev, A., and Maslov, A., 2008, "Flight Testing of DBD Plasma Separation Control System," AIAA–2008–373.

[24] Grundmann, S., Frey, M., and Tropea, C., 2009, "Unmanned Aerial Vehicle (UAV) with Plasma Actuators for Separation Control," AIAA–2009–698.

[25] Abe, T., Takizawa, Y., Sato, S., and Kimura, N., 2007, "A Parametric Experimental Study for Momentum Transfer by Plasma Actuator," AIAA–2007–187.

[26] Gregory, J.W., Enloe, C.L., Font, G.I., and McLaughlin, T., 2007, "Force Production Mechanisms of a Dielectric-Barrier Discharge Plasma Actuator," AIAA–2007–185.

[27] Schuele, C.Y. and Corke, T., 2008, "Characteristics of Single Dielectric Barrier Discharge Plasma Actuators at Sub-atmospheric Pressures," 61st Annual Meeting of the APS/DFD, San Antonio, Texas, Nov. 2008, http://meetings.aps.org/link/BAPS.2008.DFD.ET.9

[28] Takagaki, M., Isono, S., Nagai, H., and Asai, K., 2008, "Evaluation of Plasma Actuator Performance in Martian Atmosphere for Applications to Mars airplanes," AIAA–2008–3762.

[29] Benard, N., Balcon, N., and Moreau, E., 2008, "Electric Wind Produced by a Surface Dielectric Barrier Discharge Operating in Air at Different Pressures: Aeronautical Control Insights," J. Phys D: Appl Phys. 41 (2008) pp. 042002.

[30] Benard, N., Balcon, N., and Moreau, E., 2008, "Electric Wind Produced by a Single Dielectric Barrier Discharge Actuator Operating in Atmospheric Flight Conditions: Pressure Outcome," AIAA–2008–3792.

[31] Valerioti, J., and Corke, T., 2009, "Effect of Dielectric Properties on Functional Relationship between Plasma Initiation and Ambient Pressure," 62nd Annual Meeting of the APS/DFD, Minneapolis, MN, Nov 2009. http://meetings.aps.org/link/BAPS.2009.DFD.GD.1

[32] Font, G.I., Enloe, C.L., Newcomb, J.Y., Teague, A.L., Vasso, A.R., and McLaughlin, T.E., 2010, "Effects of Oxygen Content on the Behavior of the Dielectric Barrier Discharge Aerodynamic Plasma Actuator," AIAA–2010–545.

[33] Benard, N., and Moreau, E., 2010, "Effects of Altitude on the Electromechanical Characteristics of Dielectric Barrier Discharge Plasma Actuators," AIAA–2010–4633.

[34] Valerioti, J.A., 2010, "Pressure Dependence of Plasma Actuated Flow Control," MS Thesis, University of Notre Dame, Indiana.

[35] Valerioti, J., and Corke, T., 2010, "Pressure Dependence of Plasma Actuated Flow Control," 63rd Annual Meeting of the APS Division of Fluid Dynamics, Long Beach, California, November 2010. http://meetings.aps.org/link/BAPS.2010.DFD.QJ.4 Also: Submitted for AIAA Journal.

[36] Lytle, J.K., 2000, "The Numerical Propulsion Simulation: An Overview," NASA/TM—2000-209915.

[37] Jones, S.M., 2007, "An Introduction to Thermodynamic Performance Analysis of Aircraft Gas Turbine Engine Cycles Using the Numerical Propulsion System Simulation Code," NASA/TM—2007-214690.

[38] Tong, M.T., Naylor, B.A., 2008, "An Object-Oriented Computer Code for Aircraft Engine Weight Estimation," ASME Paper No. GT2008-50062.

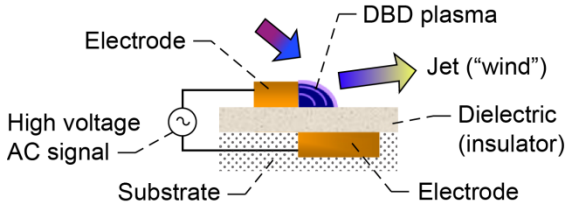

Figure 1. Schematic of a DBD plasma actuator.

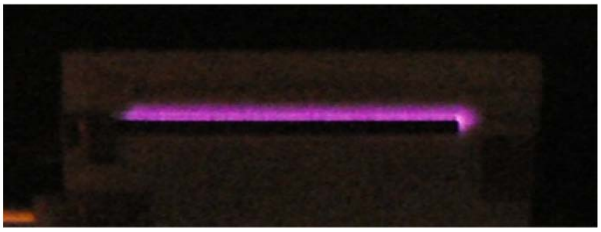

Figure 2. Top view of typical DBD discharge (Alumina dielectric with copper electrodes, NASA GRC experiment).

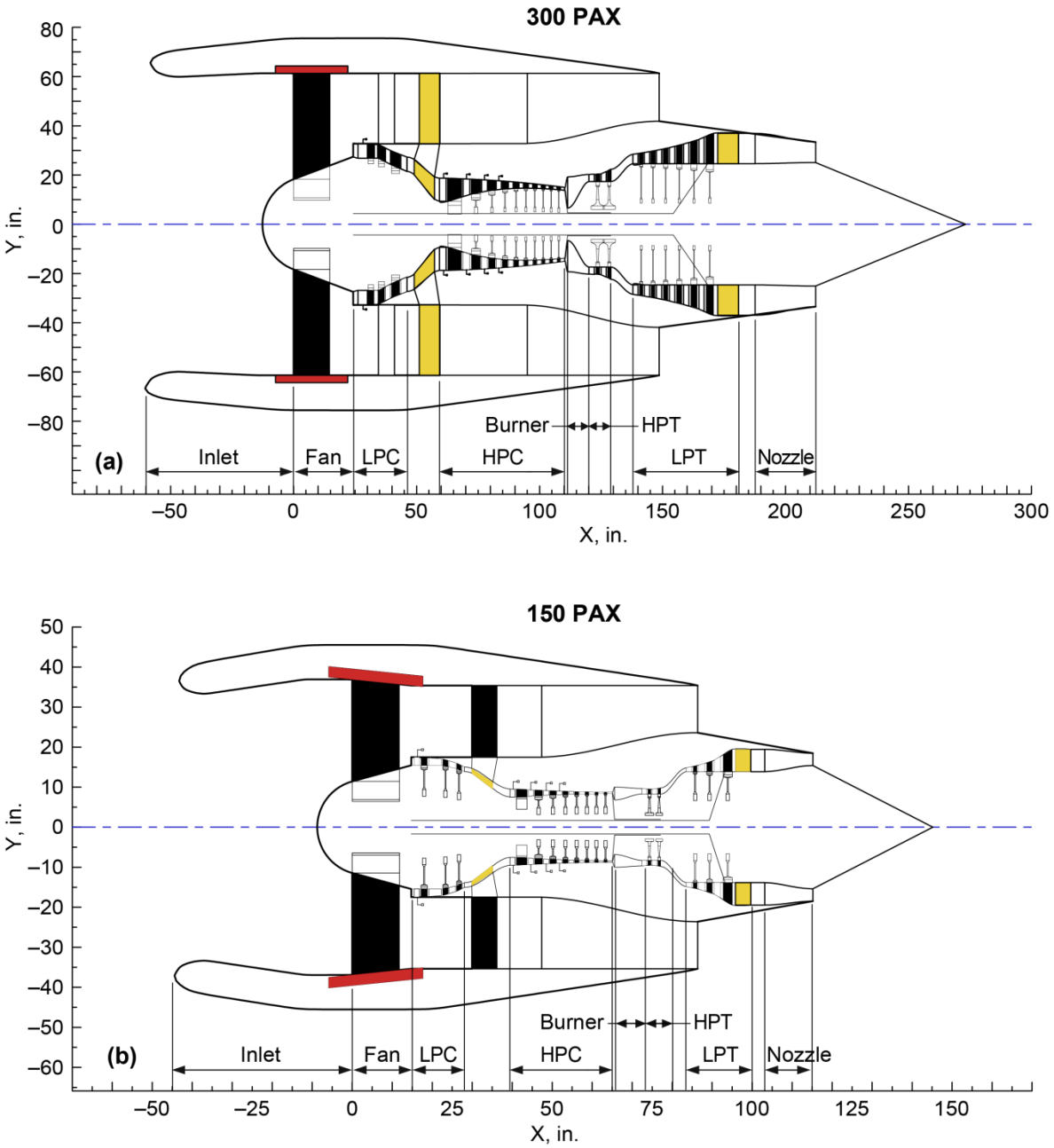

Figure 3. Schematics of four engine models. (a) 300 PAX. (b) 150 PAX.

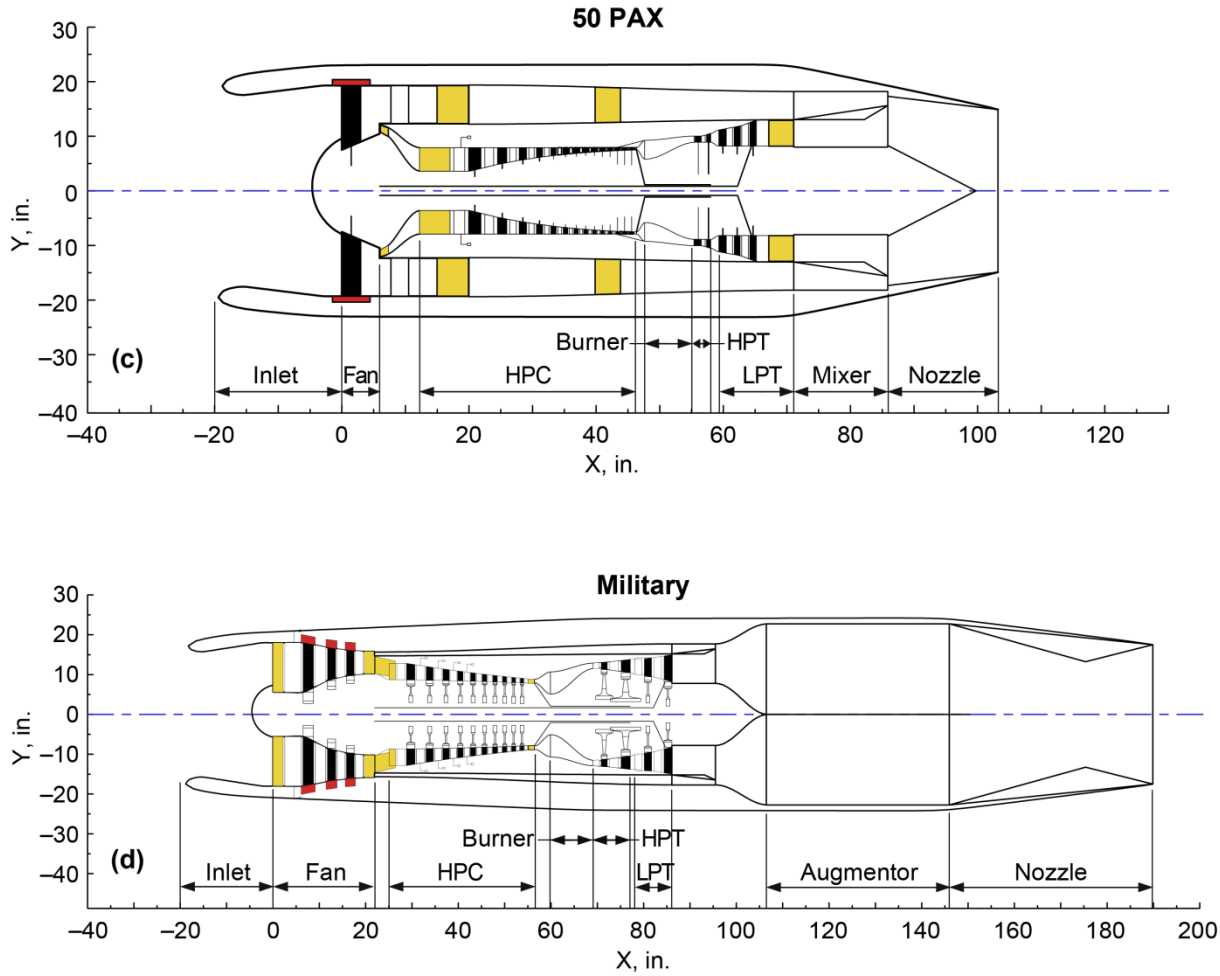

Figure 3. Schematics (concluded). (c) 50 PAX. (d) Military.

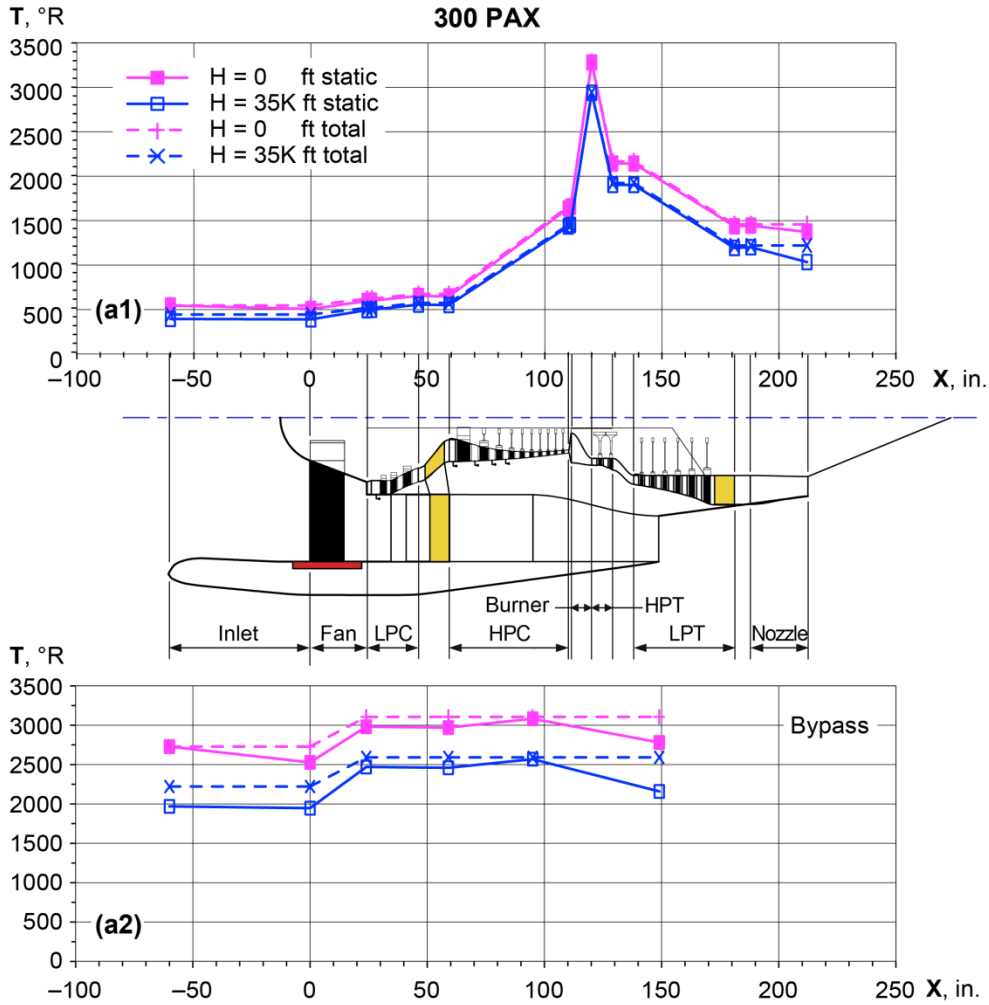

Figure 4a. 300 PAX engine–static and total temperatures. (a1) Core flow-path. (a2) Bypass.

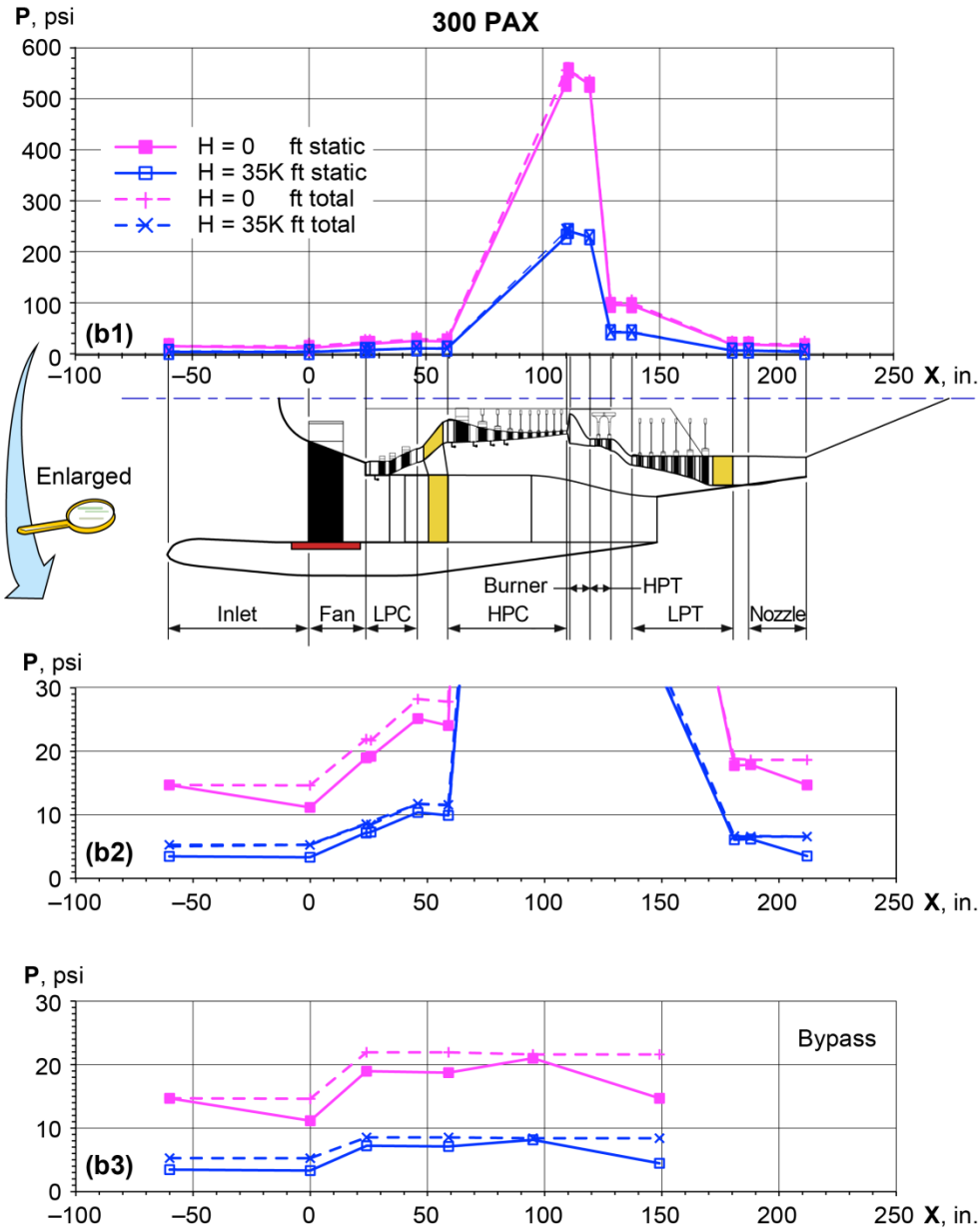

Figure 4b. 300 PAX engine–static and total pressures. (b1) Core flow-path full-pressure scale. (b2) Enlargement of (b1). (b3) Bypass.

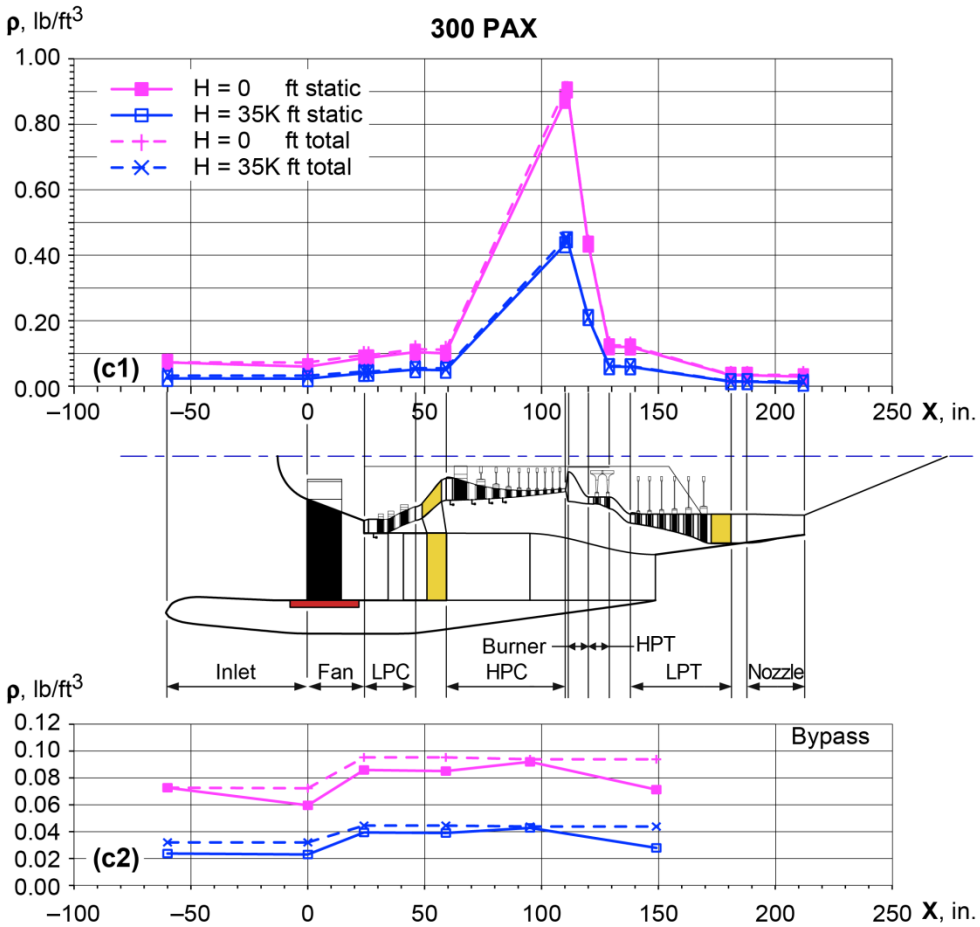

Figure 4c. 300 PAX engine–static and total densities. (c1) Core flow-path. (c2) Bypass.

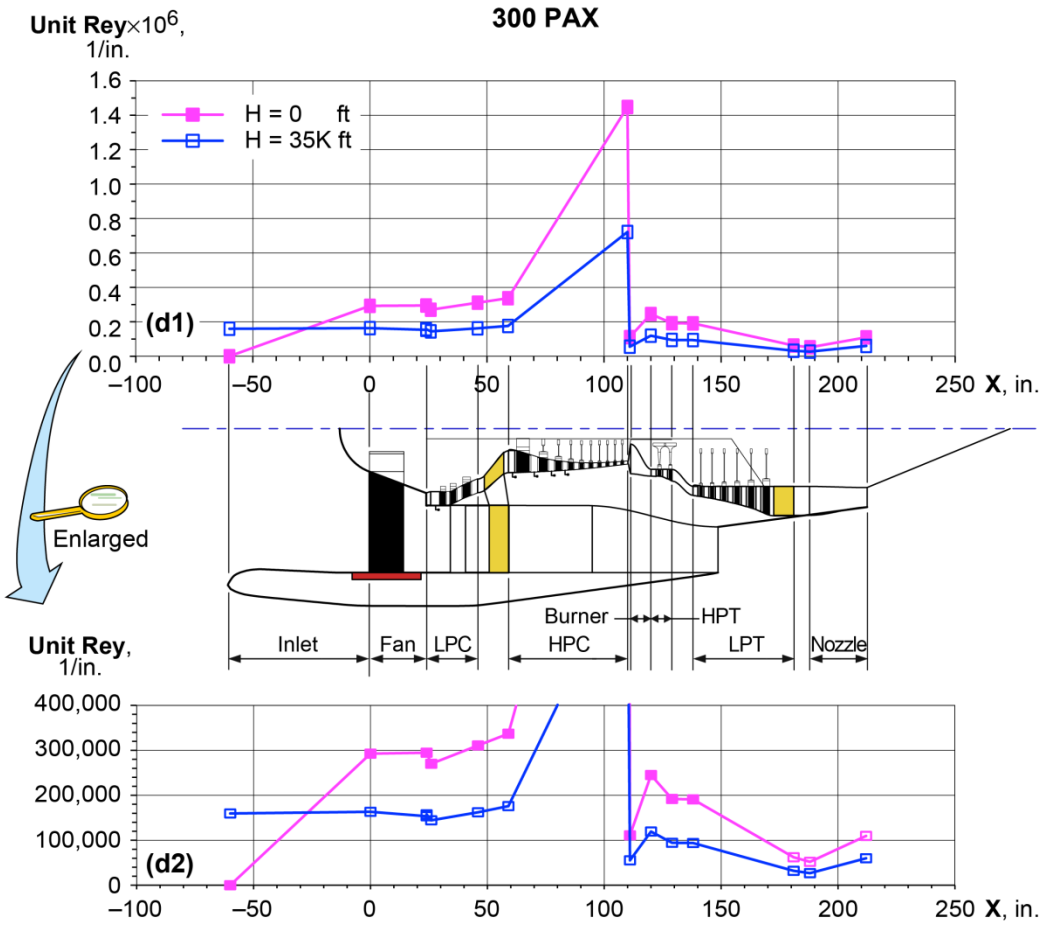

Figure 4d. 300 PAX (d1) unit Reynolds number in core flow-path. Full unit Reynolds number scale. (d2) Enlargement.

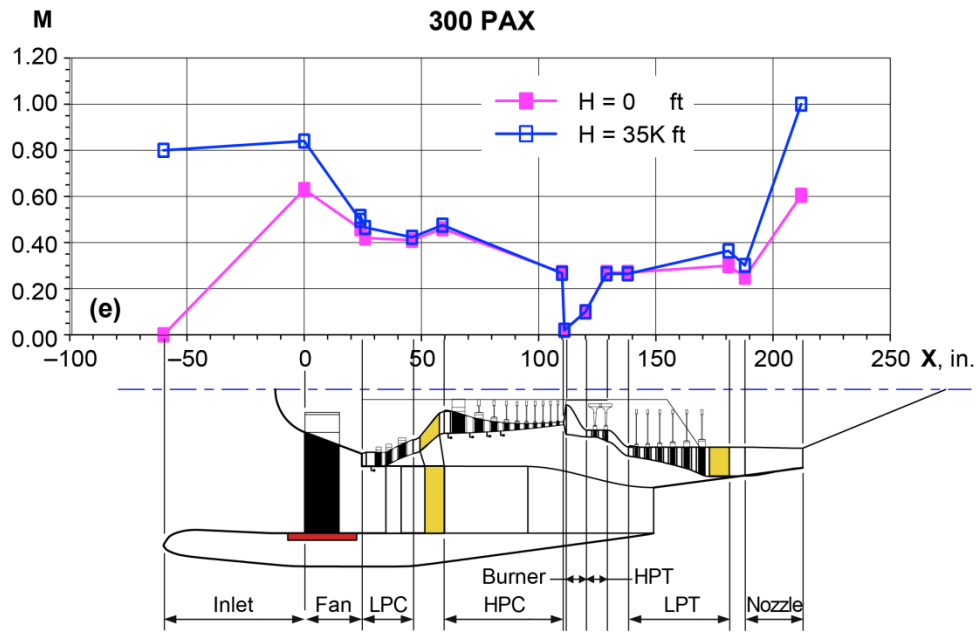

Figure 4e. 300 PAX engine–Mach number in the core flow-path.

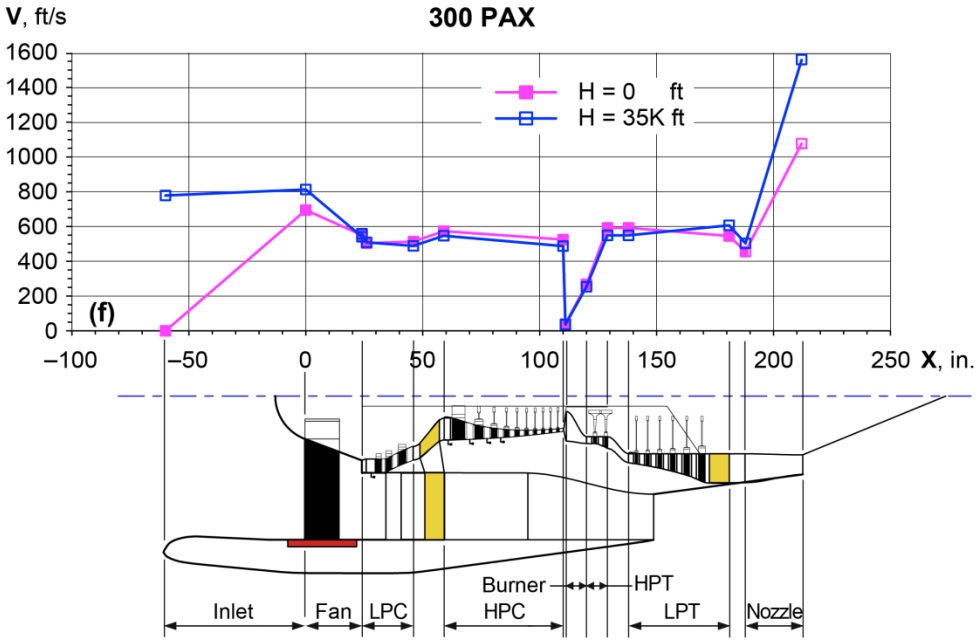

Figure 4f. 300 PAX engine–Velocity in the core flow-path.

Figure 4. Engine data for 300 PAX engine model (a) Temperatures. (b) Pressures. (c) Density. (d) Unit Reynolds number. (e) Mach number, (f) Velocity, for sea-level takeoff and 35,000 ft cruise.

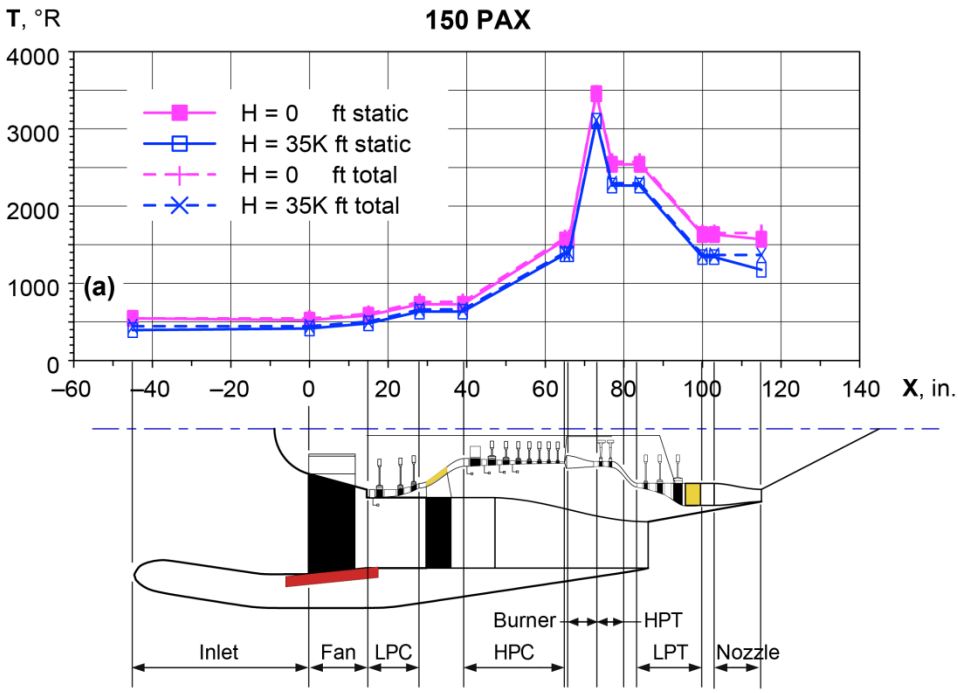

Figure 5a. 150 PAX engine–static and total temperatures.

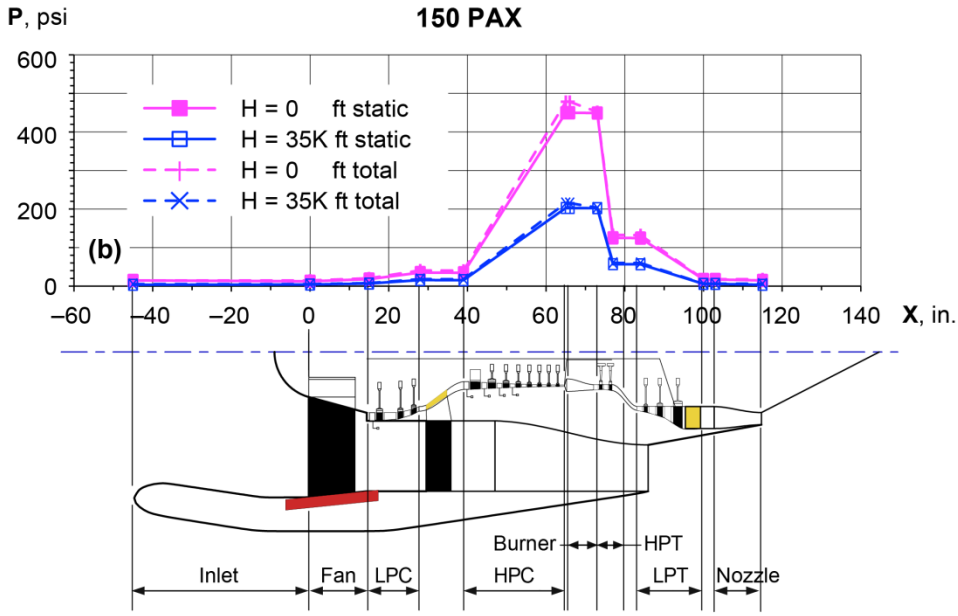

Figure 5b. 150 PAX engine–static and total pressures.

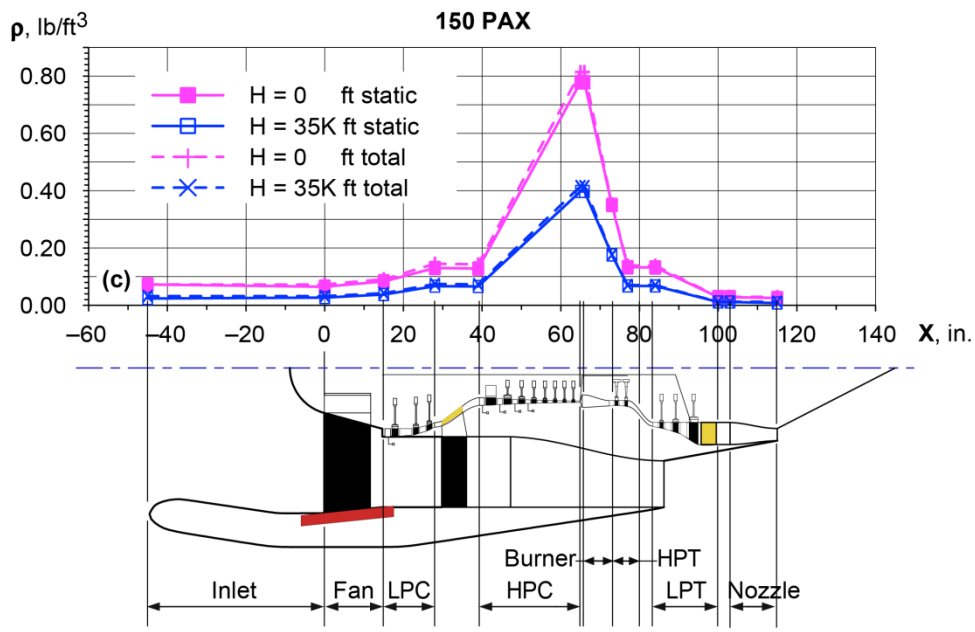

Figure 5c. 150 PAX engine–static and total densities.

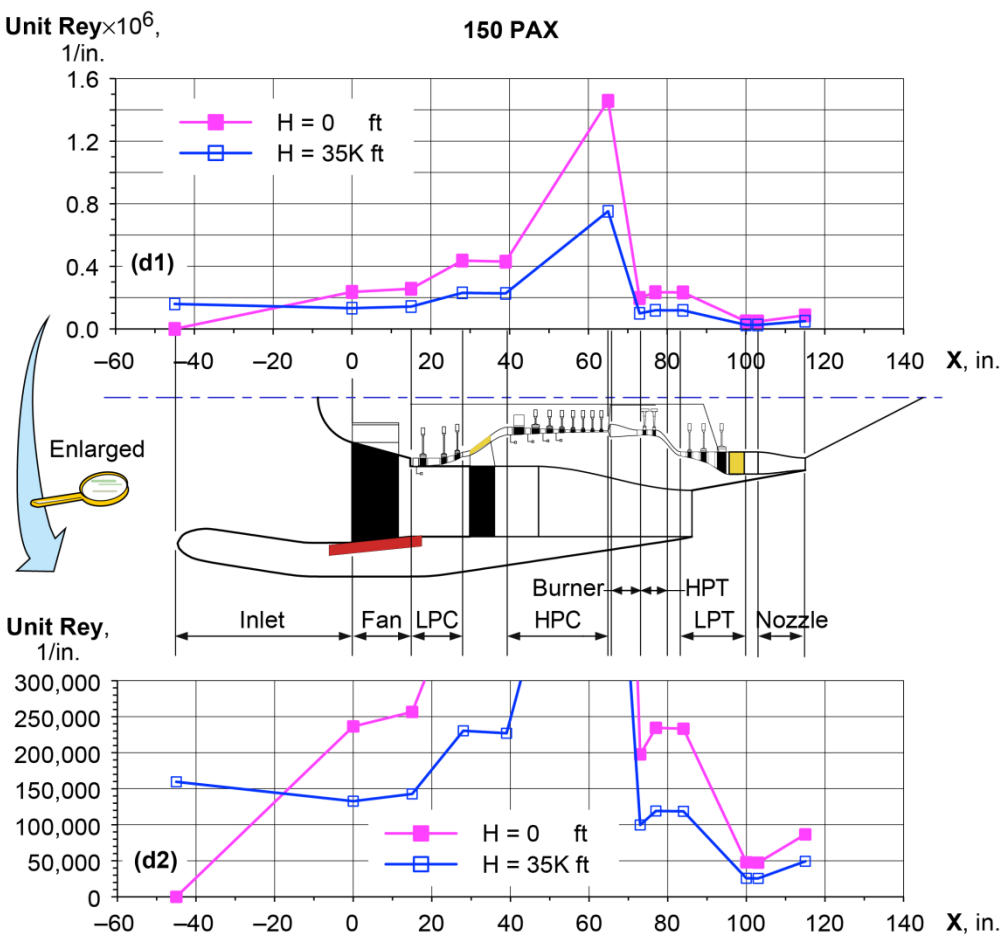

Figure 5d. 150 PAX engine–unit Reynolds numbers. (d1) Full unit Reynolds number scale. (d2) Enlargement.

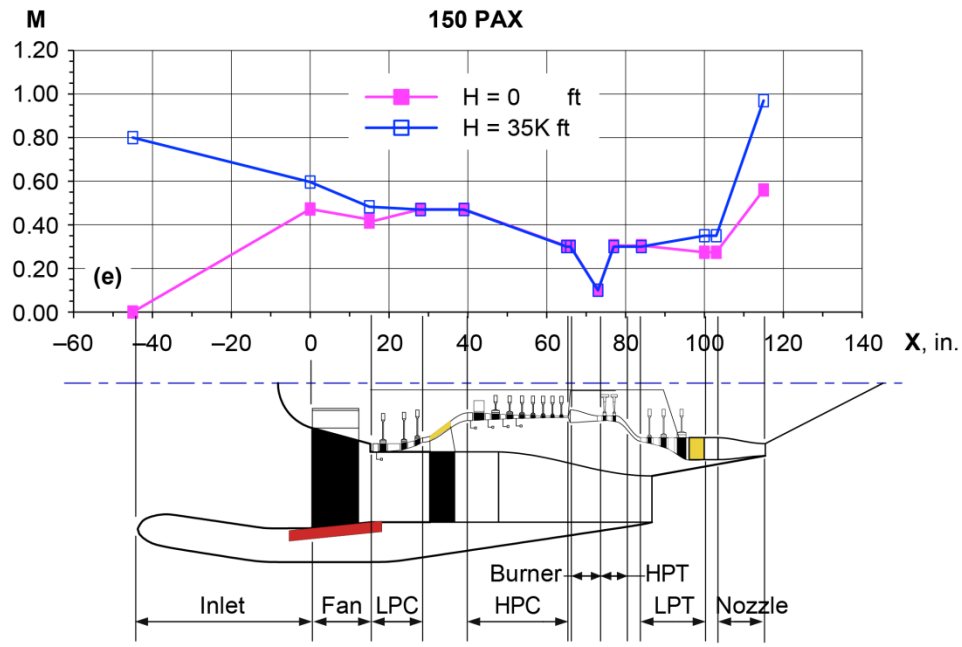

Figure 5e. 150 PAX engine–Mach number.

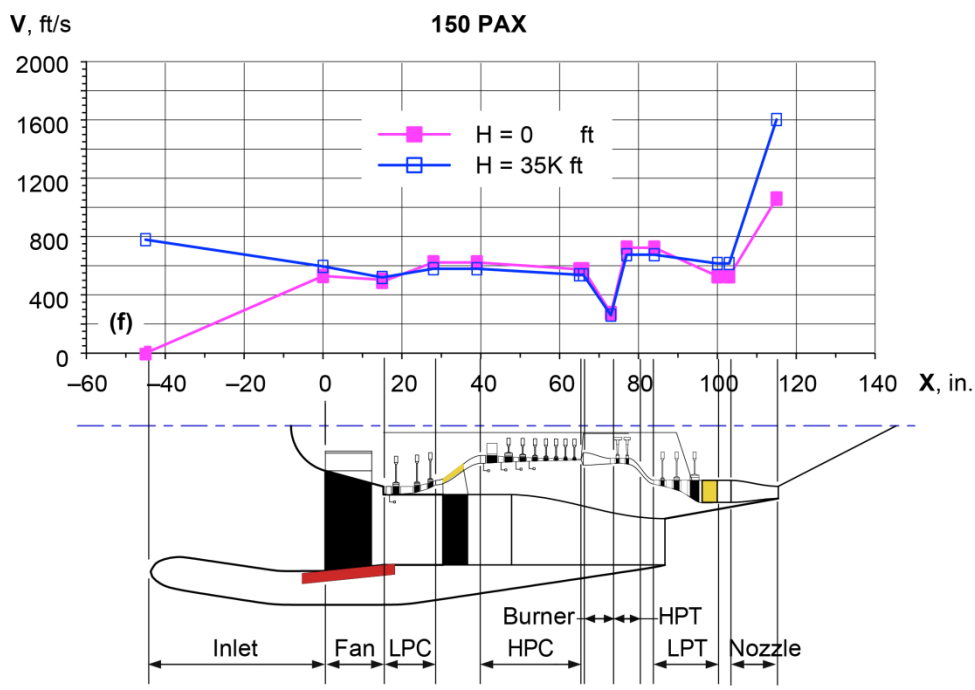

Figure 5f. 300 PAX engine–Velocity.

Figure 5. Engine data for 150 PAX engine model (a) Temperatures. (b) Pressures. (c) Densities. (d) Unit Reynolds number. (e) Mach number. (f) Velocity, for sea-level takeoff and 35,000 ft cruise.

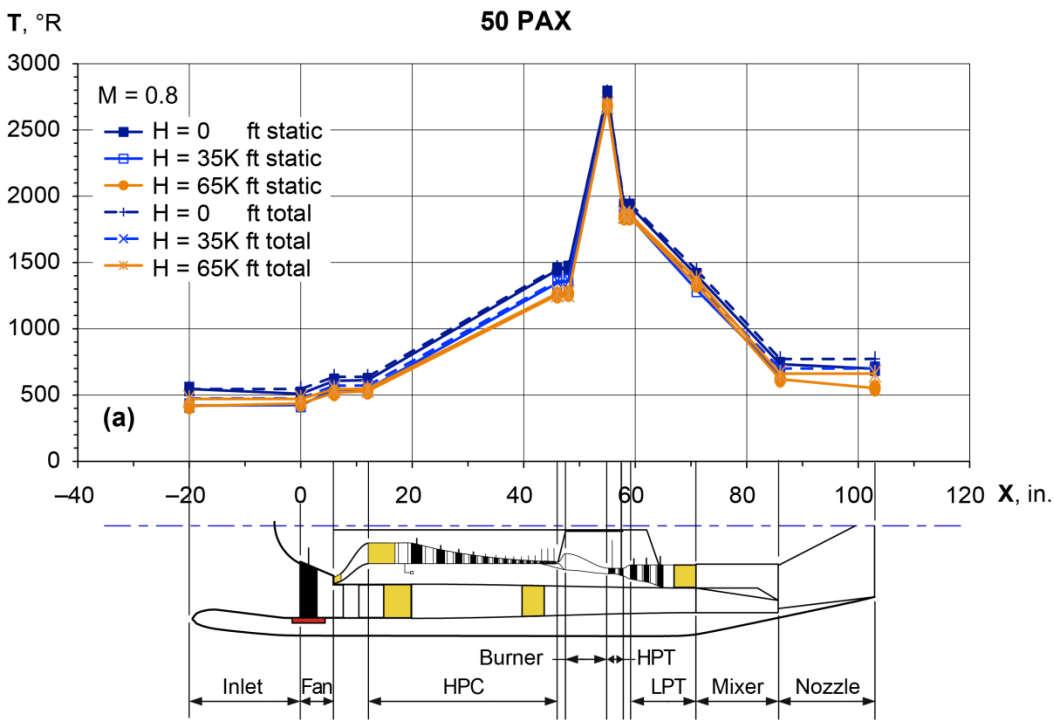

Figure 6a. 50 PAX engine–static and total temperatures, M = 0 at sea level, M = 0.8 at 35,000 ft and 65,000 ft.

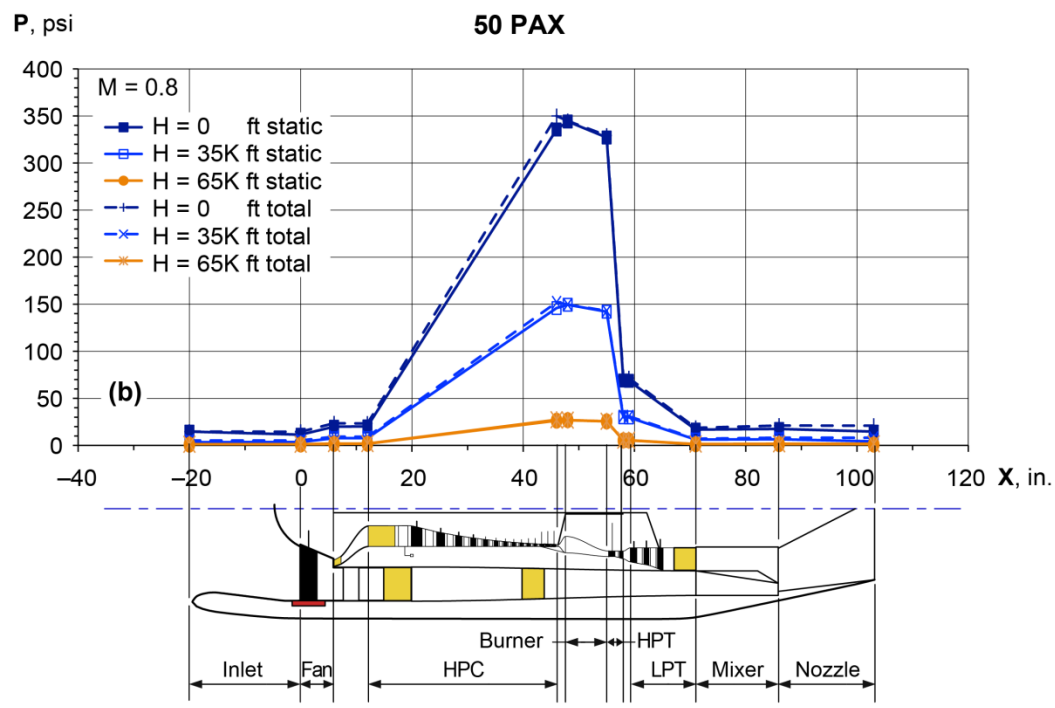

Figure 6b. 50 PAX engine–static and total pressures, M = 0 at sea level, M = 0.8 at 35,000 ft and 65,000 ft.

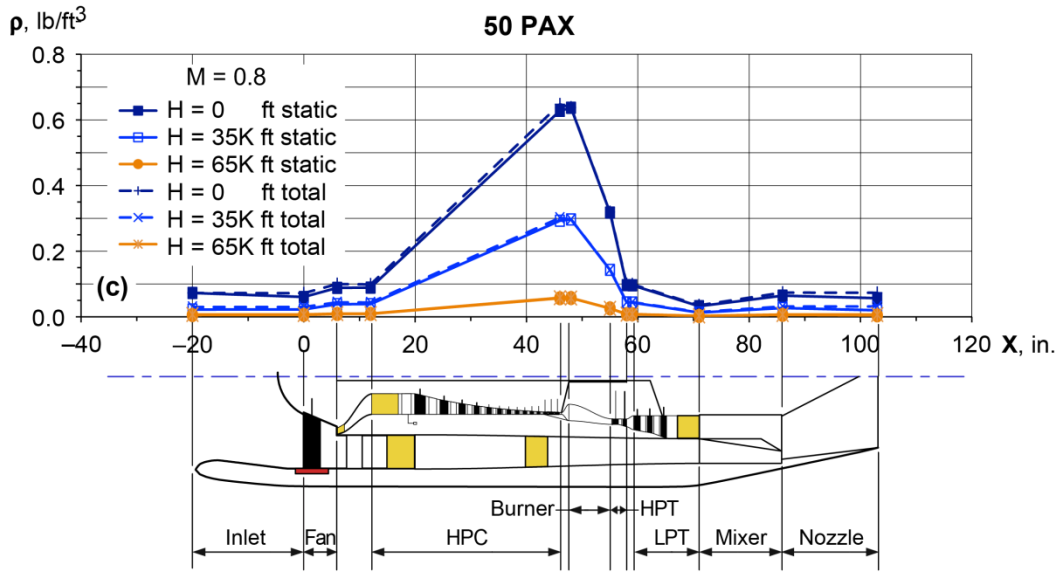

Figure 6c. 50 PAX engine–static and total densities, M = 0 at sea level, M = 0.8 at 35,000 ft and 65,000 ft.

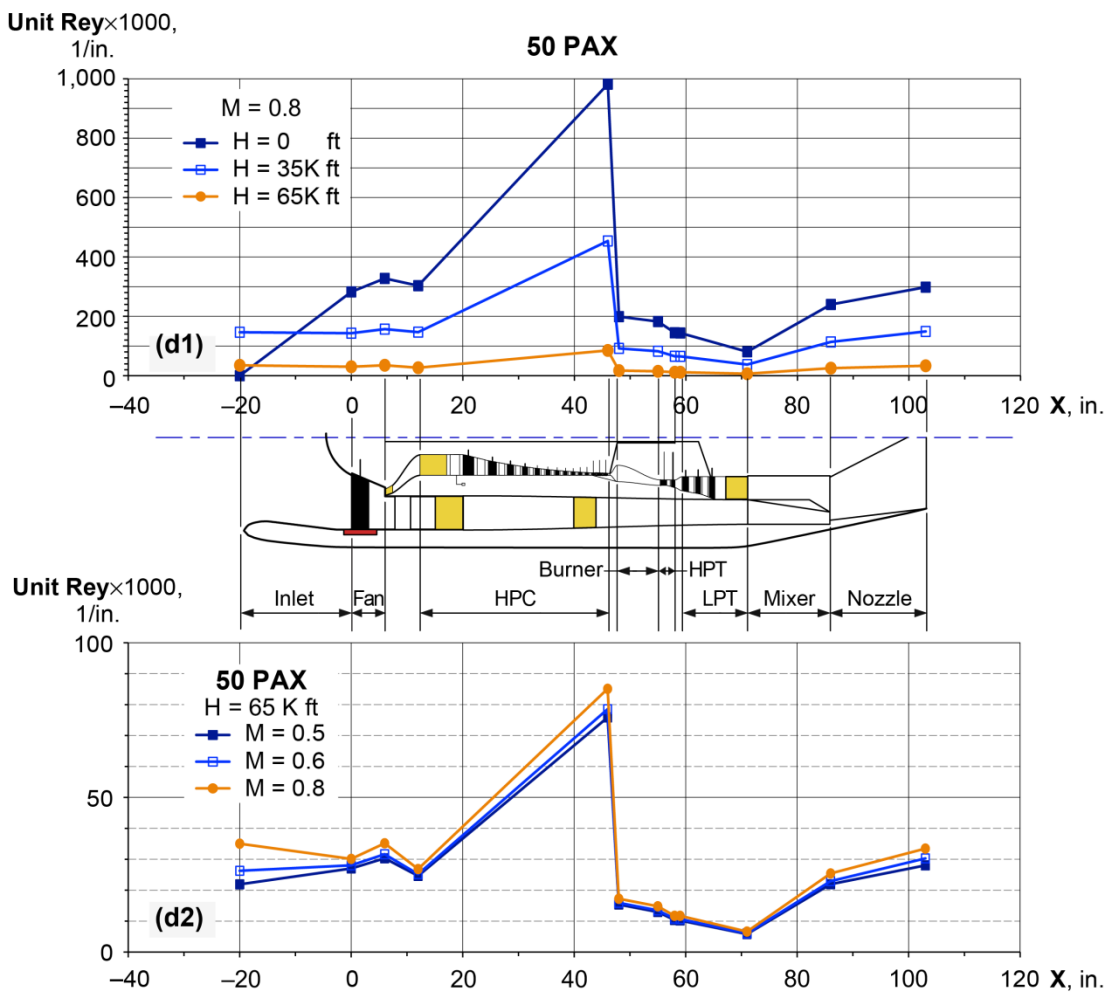

Figure 6d. 50 PAX engine–unit Reynolds number. (d1) For M = 0 at sea level, M = 0.8 at 35,000 ft and 65,000 ft. (d2) For M = 0.5, 0.6, and 0.8 at 65,000 ft.

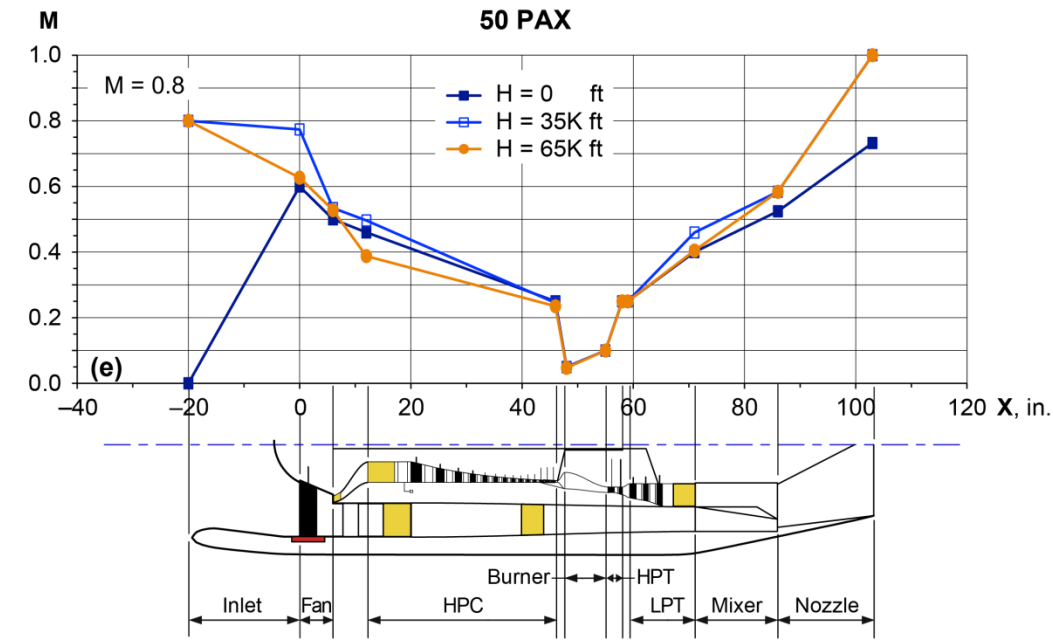

Figure 6e. 50 PAX engine–Mach number, M = 0 at sea level, M = 0.8 at 35,000 ft and 65,000 ft.

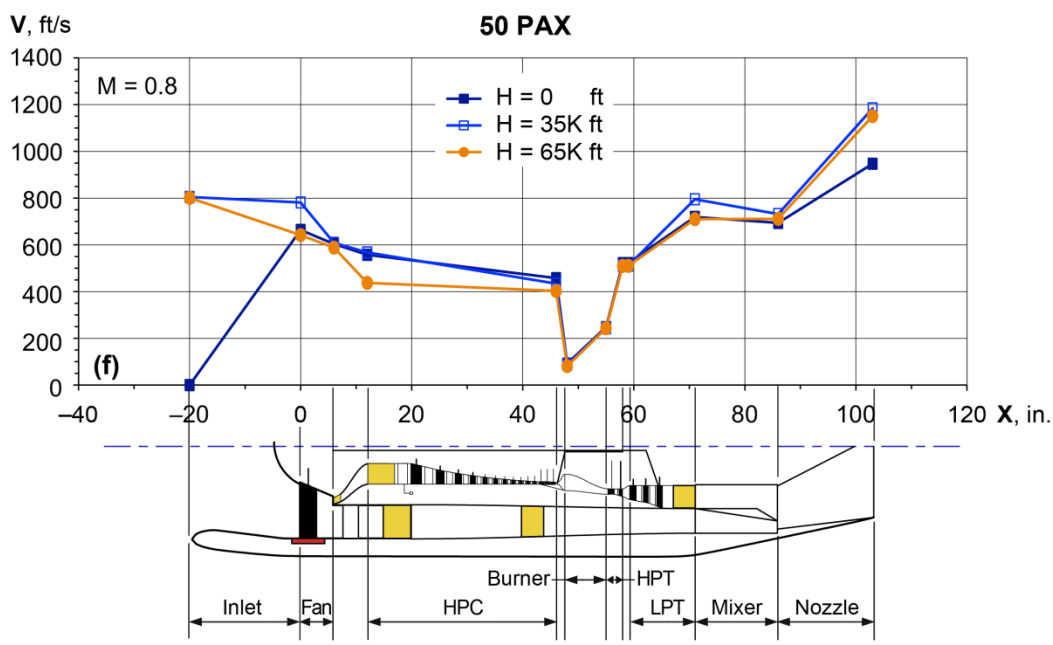

Figure 6f. 50 PAX engine–Velocity, M = 0 at sea level, M = 0.8 at 35,000 ft and 65,000 ft.

Figure 6. Engine data for 50 PAX engine model (a) Temperatures. (b) Pressures. (c) Densities. (d) Unit Reynolds number. (e) Mach number. (f) Velocity, for sea-level takeoff and 35,000 ft and 65,000 ft cruise.

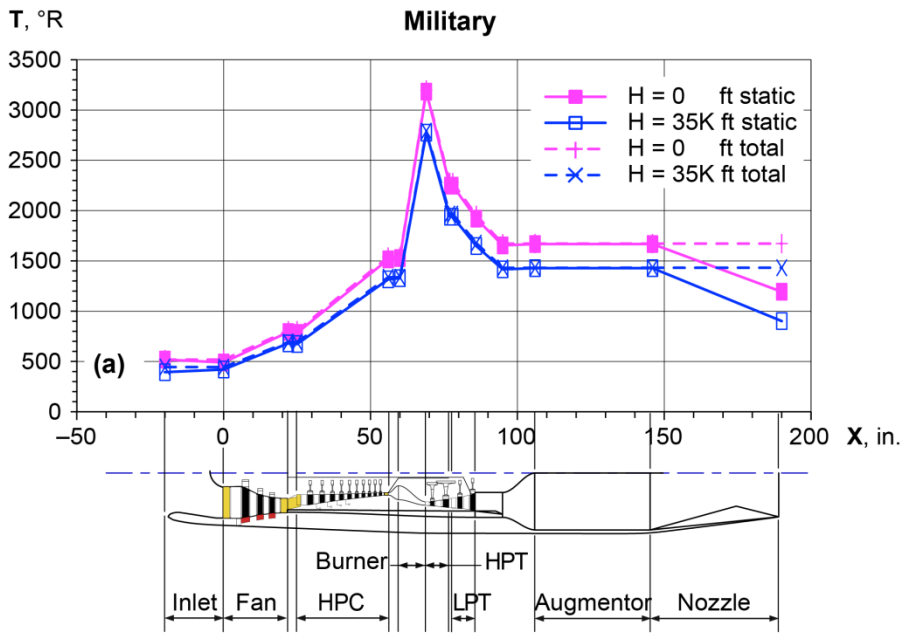

Figure 7a. Military jet fighter engine–static and total temperatures.

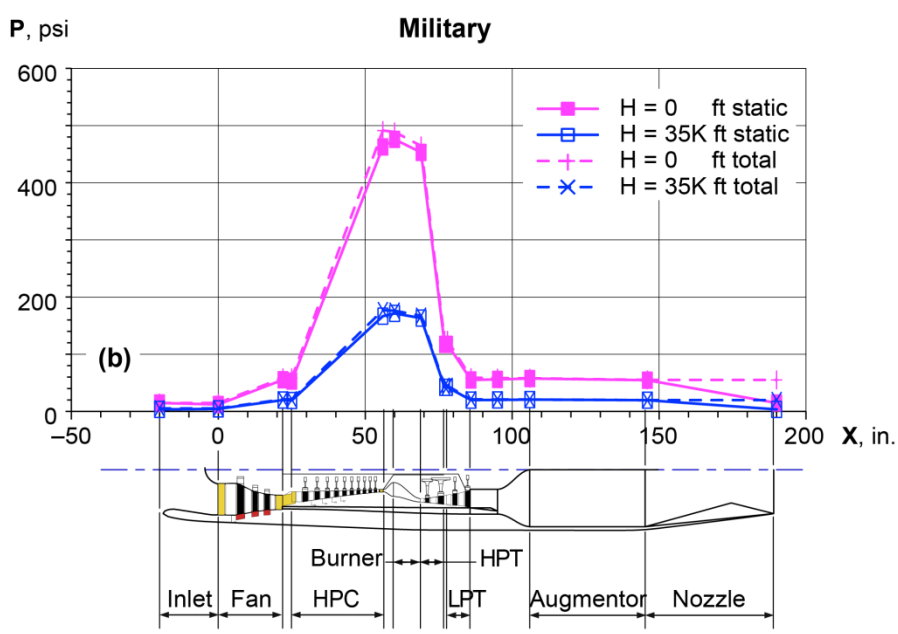

Figure 7b. Military jet fighter engine–static and total pressures.

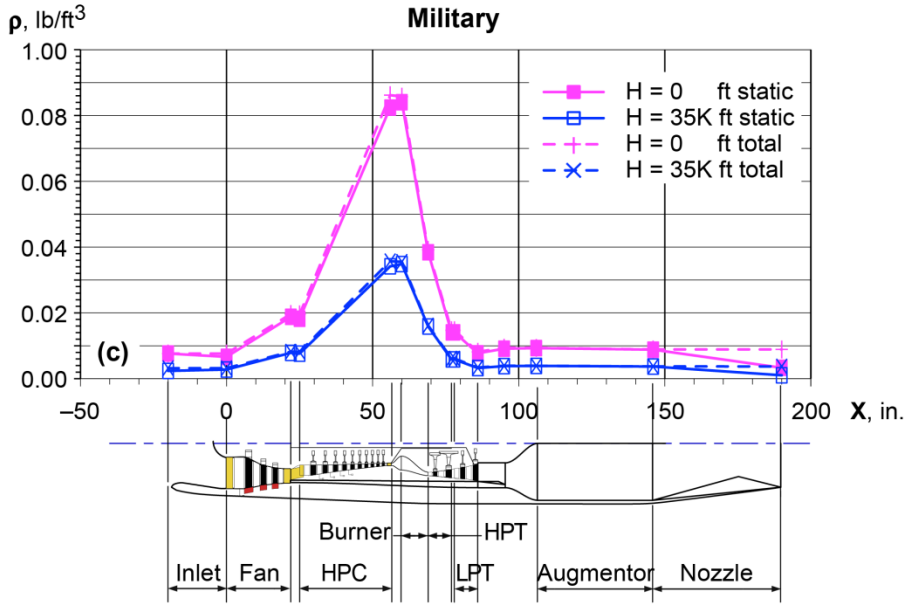

Figure 7c. Military jet fighter engine–static and total densities.

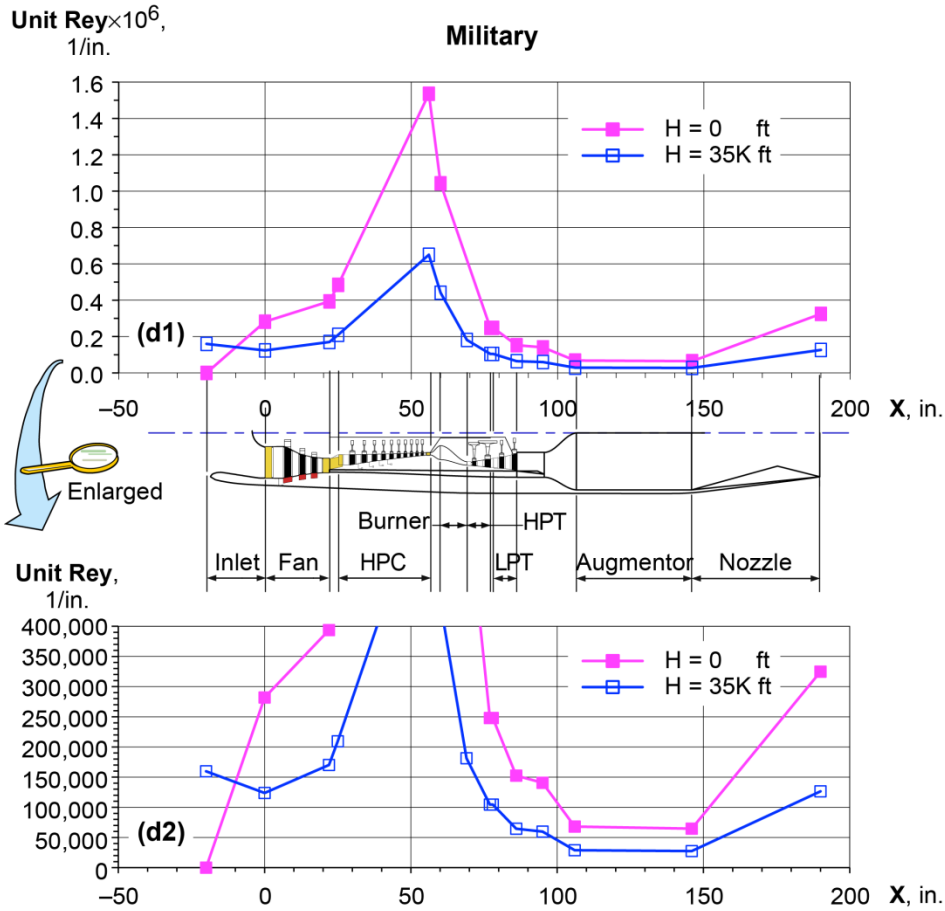

Figure 7d. Military jet fighter engine–unit Reynolds number. (d1) Full unit Reynolds number scale. (d2) Enlargement.

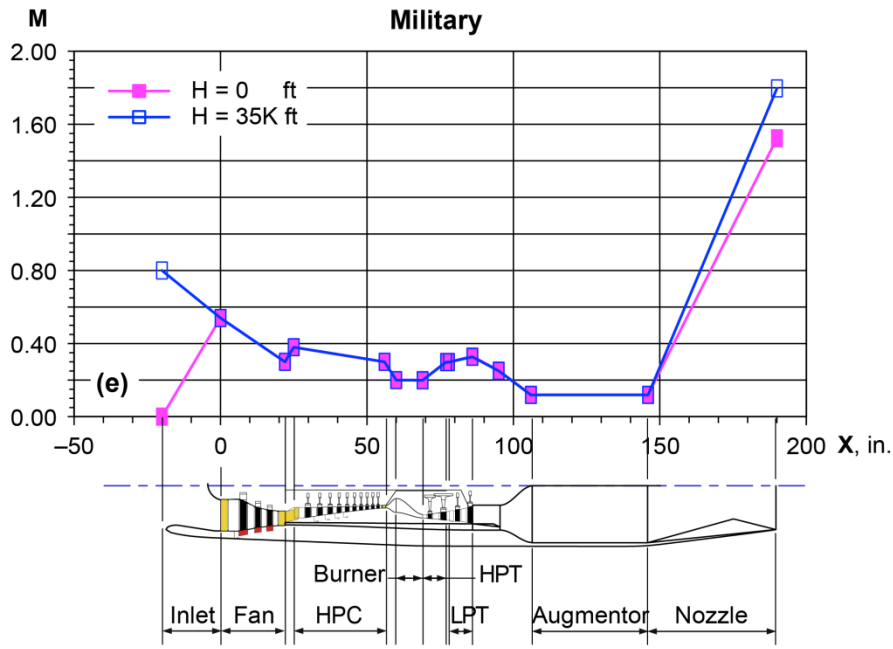

Figure 7e. Military jet fighter engine–Mach number.

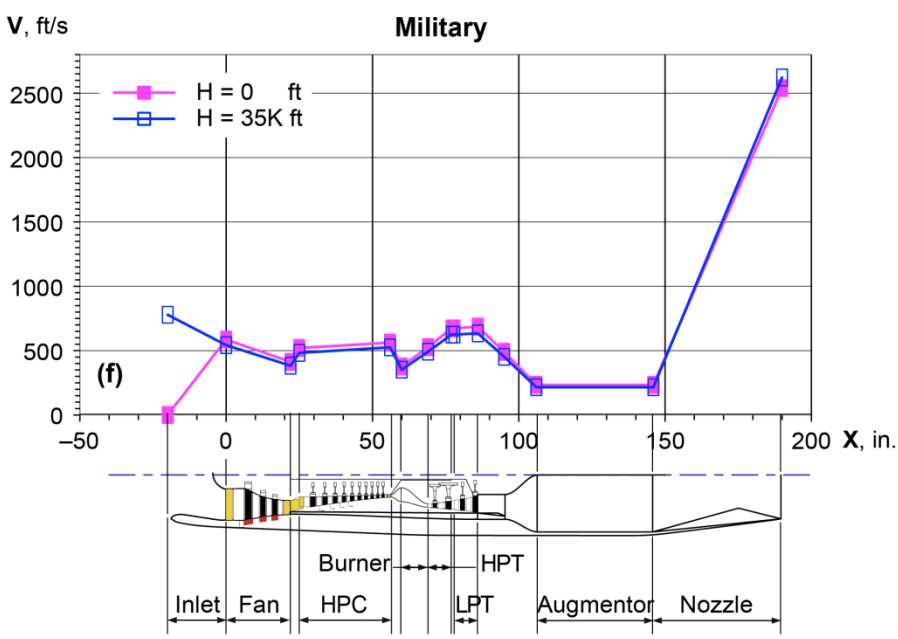

Figure 7f. Military jet fighter engine–Velocity.

Figure 7. Military jet fighter engine model (a) Temperatures. (b) Pressures. (c) Densities. (d) Unit Reynolds number. (e) Mach number. (f) Velocity, for sea-level takeoff and 35,000 ft cruise.

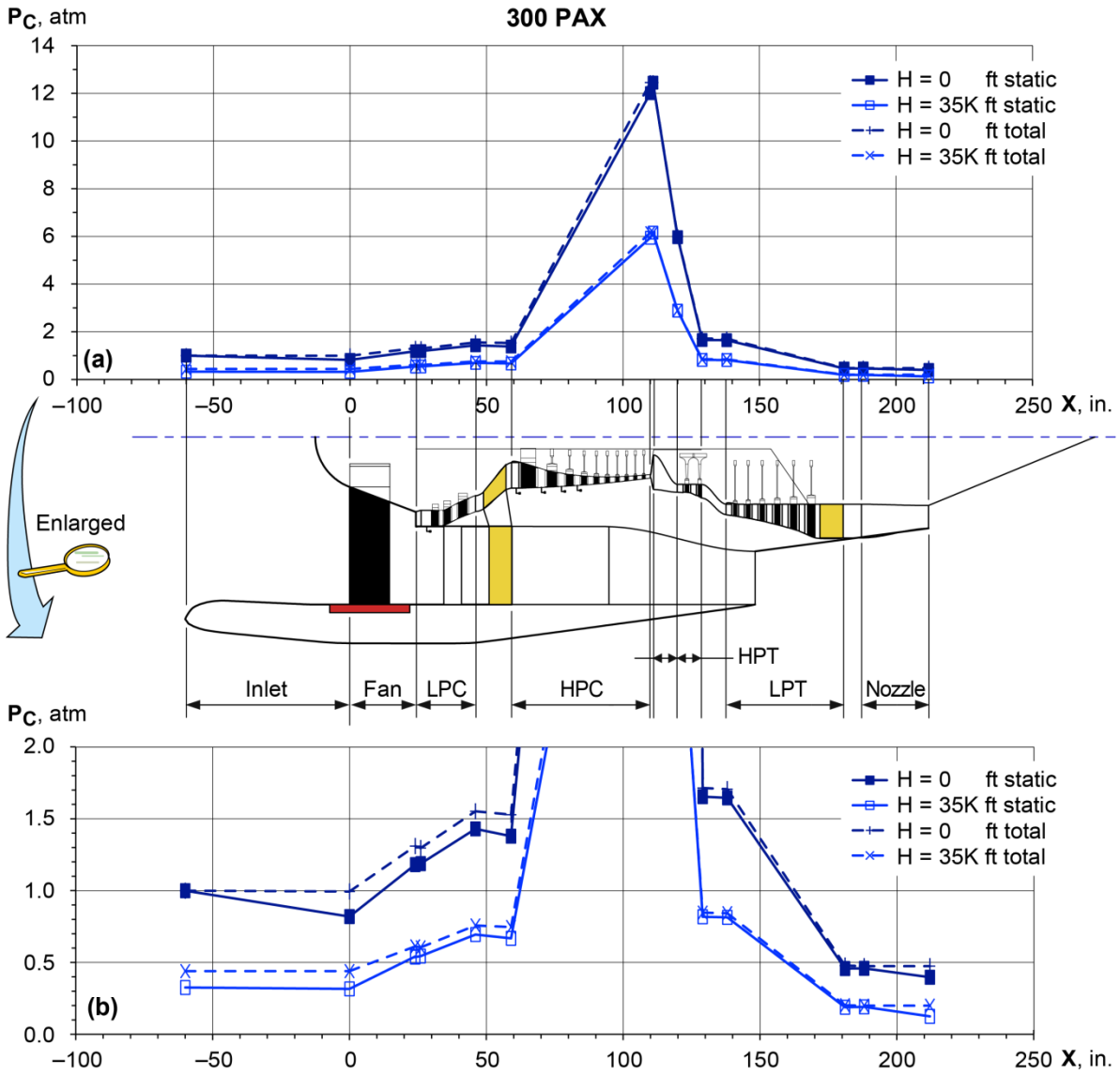

Figure 8a. 300 PAX engine–chamber pressure. (a) Full scale plot. (b) Enlargement of (a).

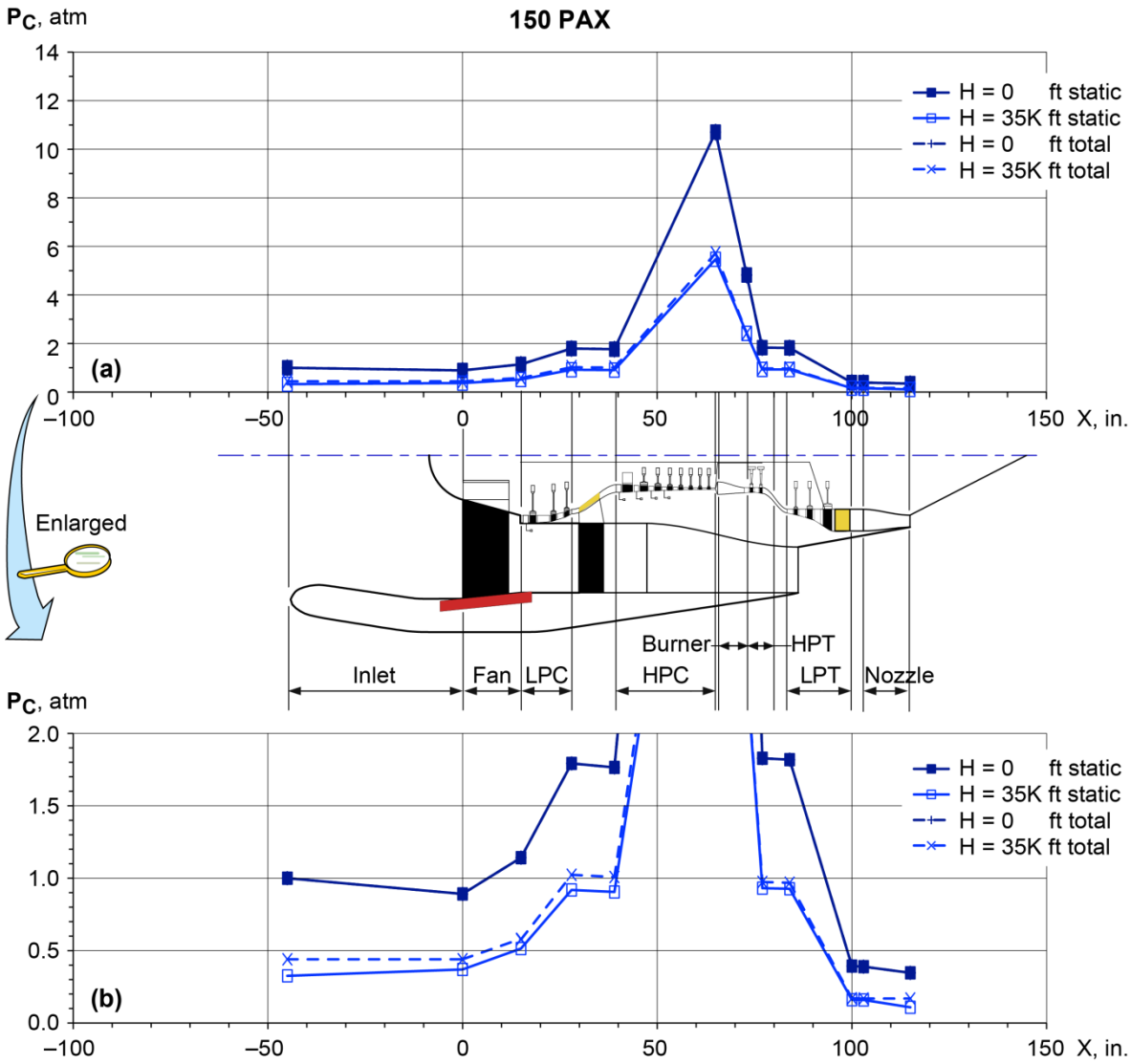

Figure 8b. 150 PAX engine–chamber pressure. (a) Full scale plot. (b) Enlargement of (a).

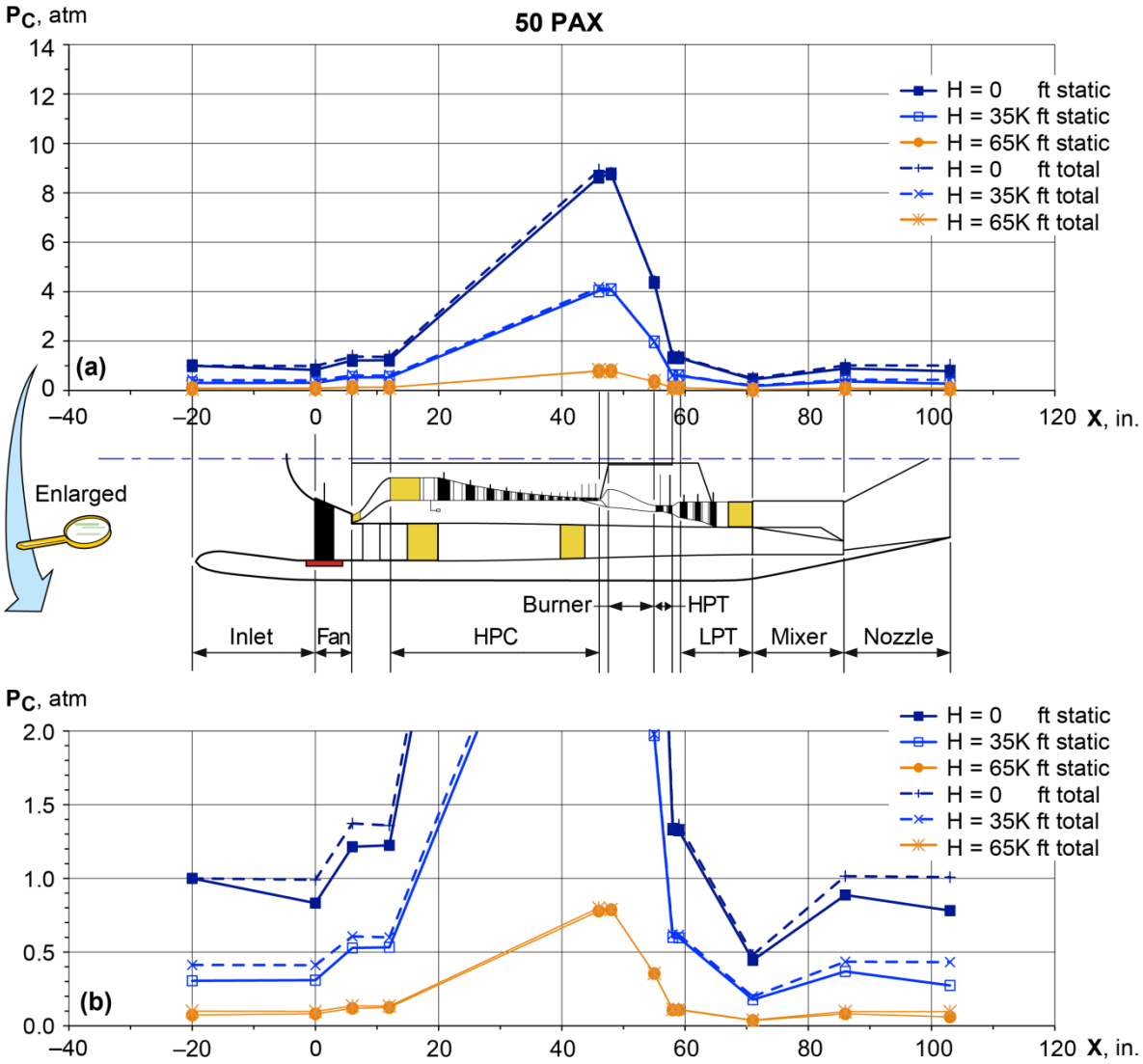

Figure 8c. 50 PAX engine–chamber pressure. (a) Full scale plot. (b) Enlargement of (a).

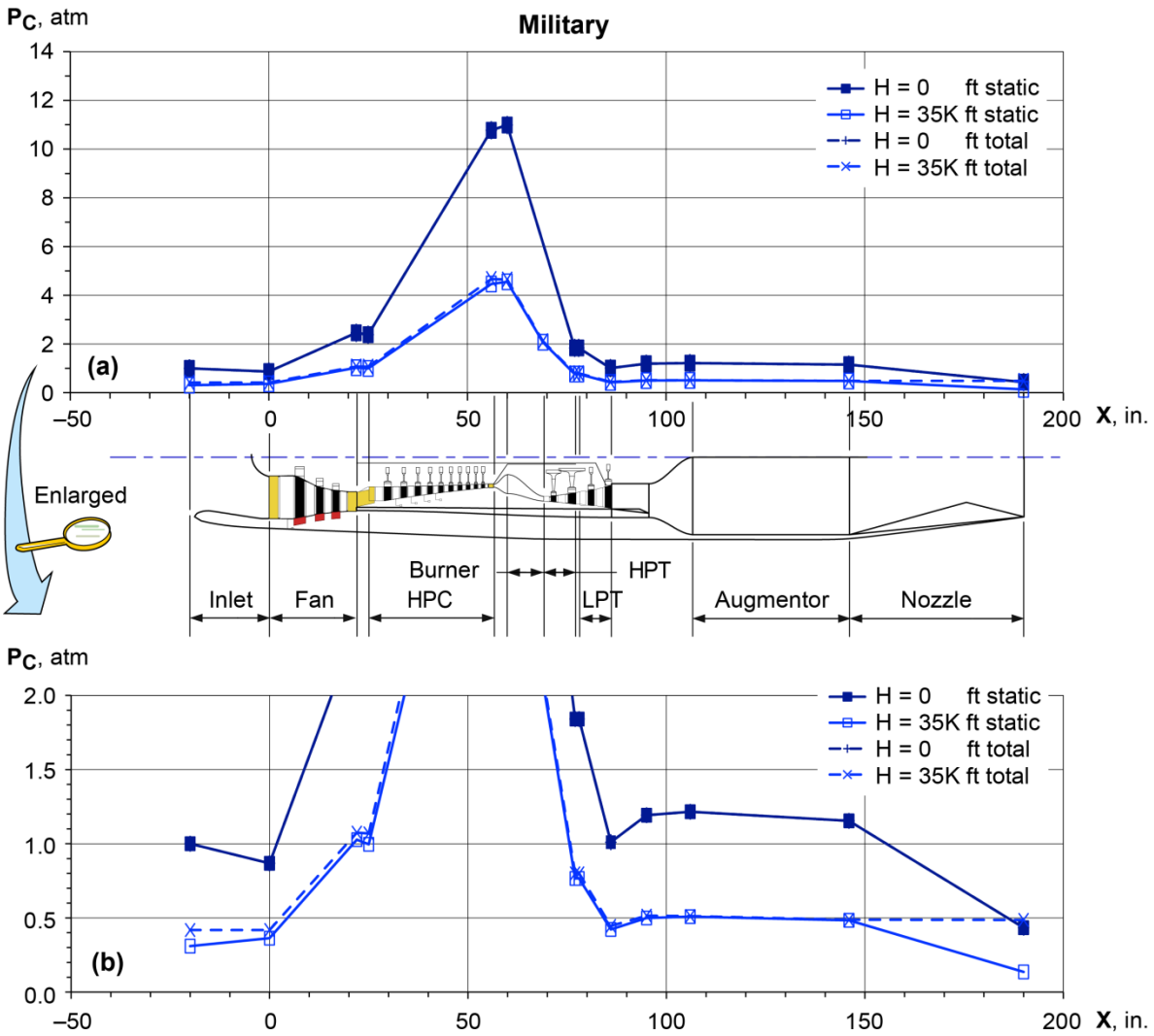

Figure 8d. Military engine–chamber pressure. (a) Full scale plot. (b) Enlargement of (a).

Table 1. Parameters of four engine models.

Engine	Thrust	Weight	OPR		BPR
	At Sea-level static	Bare Engine	Overall Pressure Ratio		Bypass Ratio
	(lbf)	(lb)	At Sea-level	At 35k ft	At 35k ft
300PAX	86,700	18,400	37.8	45.7	8.3
150PAX (future)	23,400	5,100	33.5	42.0	14.3
50PAX	7,600	1,300	23.5	28.4	5.3
Military	18,500	3,800	33.4	33.6	0.4

Table 2. Axial coordinates of engine model components.

300 PAX		**150 PAX**		**50 PAX**		**Military**	
X, in.	**Component outflow plane**	**X, in.**	**Component outflow plane**	**X, in.**	**Component outflow plane**	**X, in.**	**Component outflow plane**
Core		**Core**		**Core**		**Core**	
–60	Ambient	–45	Ambient	–20	Ambient	–20	Ambient
0	Inlet	0	Inlet	0	Inlet	0	Inlet
24	Fan	15	Fan	6	Fan	22	Fan
24	Splitter	15	Splitter	12	Duct	25	Duct
26	Duct	15	Duct	46	HPC	56	HPC
46	LPC	28	LPC	48	Duct	60	Duct
59	Duct	39	Duct	55	Burner	69	Burner
110	HPC	65	HPC	58	HPT	77	HPT
111	Duct	66	Duct	59	Duct	78	TDuct
120	Burner	73	Burner	71	LPT	86	LPT
129	HPT	77	HPT	86	Mixer	95	Mixer
138	Duct	84	Duct	103	Nozzle	106	Duct
181	LPT	100	LPT	**Bypass**		146	Augmentor
188	Duct	103	Duct	–20	Ambient	190	Nozzle
212	Core Nozzle	115	Core Nozzle	0	Inlet	**Bypass**	
Bypass		**Bypass**		6	Fan	–20	Ambient
–60	Ambient	–45	Ambient	71	Duct	0	Inlet
0	Inlet	0	Inlet	86	Duct	**22**	Fan
24	Fan	15	Fan			86	Duct
24	Splitter	15	Splitter			95	Mixer
59	Bypass EGV	30	Bypass EGV				
95	Duct	47	Duct				
149	Bypass Nozzle	86	Bypass Nozzle				